Complementary cognitive roles for D2-MSNs and D1-MSNs in interval timing

R. Austin Bruce[1], Matthew A. Weber[1], Alexandra S. Bova[1], Rachael A. Volkman[1], Casey E. Jacobs, Kartik Sivakumar[1], Young-cho Kim[1], Rodica Curtu[2,3], Nandakumar S. Narayanan[1,3]

[1]Department of Neurology, University of Iowa, [2]Department of Mathematics, University of Iowa, and [3]The Iowa Neuroscience Institute

***Corresponding Author**
Nandakumar Narayanan
nandakumar-narayanan@uiowa.edu
169 Newton Road
Pappajohn Biomedical Discovery Building—5336
University of Iowa, Iowa City, 52242
319-353-5698

Abstract

Striatal pathways control motivation and movement; however, their role in cognition is unclear. We studied dorsomedial striatal cognitive processing during interval timing, an elementary cognitive task that requires mice to estimate intervals of several seconds. Interval timing involves working memory for temporal rules and attention to the passage of time. We discovered that both pharmacological and optogenetic disruptions of D2-dopamine receptor-expressing medium spiny neurons (D2-MSNs) or D1-dopamine receptor-expressing MSNs (D1-MSNs) delayed timing. Disrupting D2-MSNs or D1-MSNs did not affect task-specific movements. Furthermore, pharmacological blockade of D2-dopamine receptors or D1-dopamine receptors degraded dorsomedial MSN temporal encoding. We compared the timing-related firing of optogenetically-tagged D2-MSNs and D1-MSNs. Strikingly, we found that D2-MSNs and D1-MSNs exhibited opposite dynamics over temporal intervals despite similar effects of D2-MSN and D1-MSN disruptions. MSN dynamics helped construct and constrain a four-parameter drift-diffusion computational model that captured interval timing behavior and D2-MSN and D1-MSN perturbations. Despite opposing dynamics, disrupting either D2-MSNs or D1-MSNs slowed timing, implying that D2-MSNs and D1-MSNs make complementary contributions to interval timing. These data provide novel insight into basal ganglia cognitive operations beyond movement. Our findings carry implications for a broad range of human striatal diseases and for therapies targeting striatal pathways.

Introduction

The basal ganglia have been heavily studied in motor control[1–4]. These subcortical nuclei are composed of two pathways defined by medium spiny neurons (MSNs) in the striatum: the indirect pathway, defined by D2-dopamine receptor-expressing MSNs (D2-MSNs), and the direct pathway, defined by D1-dopamine receptor-expressing MSNs (D1-MSNs). It has been proposed that the indirect and direct pathways play opposing roles in movement[1,2,5–7], although recent work identified how these pathways can play more complex and complementary roles[3,4,8,9]. MSNs receive dense input from both motor and cognitive cortical areas[10–14], but the respective roles of D2-MSNs and D1-MSNs in cognitive processing are largely unknown. Understanding the cognitive basal ganglia is critical for diseases affecting the striatum such as Huntington's disease, Parkinson's disease, and schizophrenia[15–17]. Furthermore, pharmacological and brain stimulation therapies directly modulate D2-MSNs, D1-MSNs, or downstream basal ganglia structures such as the globus pallidus or subthalamic nucleus. Determining striatal pathway contributions to cognition may help avoid side effects of current treatments and inspire novel therapeutic directions.

We studied striatal D2-MSNs and D1-MSNs during an elementary cognitive task, interval timing. This task requires estimating an interval of several seconds and provides an ideal platform to study cognition in the striatum because 1) interval timing requires cognitive resources including working memory for temporal rules and attention to the passage of time[18,19]; 2) it is reliably impaired in human striatal diseases such as Huntington's disease, Parkinson's disease, and schizophrenia[16,19–22]; 3) interval timing requires nigrostriatal dopamine that modulates MSNs[23–32]; and 4) can be rigorously studied in animal models[33–35]. Past work has

shown that disrupting D2-dopamine receptors (D2s) in the dorsomedial striatum powerfully impairs interval timing[25,36–38]. D1-dopamine receptors (D1s) can also contribute to interval timing[37–39]. These observations suggest that D2-MSNs and D1-MSNs control the timing of action; however, the respective roles remain poorly delineated.

We investigated this problem with a combination of behavioral pharmacology, cell-type-specific optogenetics, neuronal ensemble recordings, and computational modeling in the dorsomedial striatum of mice. Remarkably, we found that pharmacologic and optogenetic disruption of either indirect pathway D2-MSNs or direct pathway D1-MSNs slowed timing behavior without affecting task-specific movements. Furthermore, pharmacological blockade of either D2- or D1-receptors degraded MSN ensemble temporal encoding, suggesting that both D2- and D1-MSNs are intimately involved in the temporal control of action. We optogenetically tagged D2-MSNs and D1-MSNs to compare their patterns of activity. Strikingly, despite similar effects of D2-MSN and D1-MSN disruptions, we found opposing neuronal dynamics with D2-MSNs increasing firing over an interval and D1-MSNs decreasing firing over an interval. These data helped construct and constrain a four-parameter drift-diffusion model of MSN activity. Our results provide insight into how striatal pathways encode elementary cognitive operations and elucidate how opposing D2- and D1-MSN activity exerts similar roles in the temporal control of action. These data demonstrate that D2-MSNs and D1-MSNs play complementary cognition roles and are highly relevant for understanding the pathophysiology of human diseases and therapies targeting the striatum.

RESULTS

Interval timing measures elementary cognitive processing in mice.

We investigated cognitive processing in the striatum using a mouse-optimized interval timing task[33,40]. This task requires mice to *switch* from a short to a long nosepoke response port after approximately 6 seconds. There is no external cue indicating when to switch response ports, meaning the decision to switch response ports, or the *switch time*, is an explicit time-based decision guided by the animals' internal estimate of time (Fig 1a). Interval timing is ideal for studying elementary cognitive processing in mice using pharmacology, optogenetics, and neuronal ensemble recordings (Fig 1b) of D2-MSNs and D1-MSNs (Fig 1c-d)[41], as it requires both working memory and attention, has high relevance for human disease, and requires both striatal MSNs and nigrostriatal dopamine[16,19–31,35].

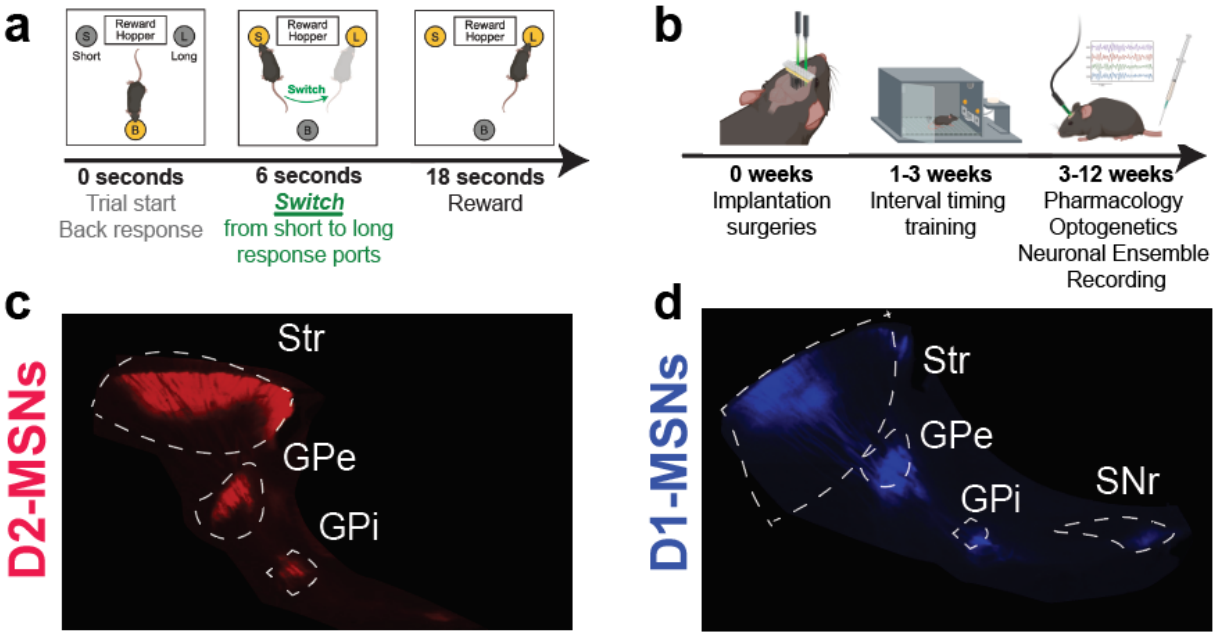

Figure 1: Interrogating striatal cognitive contributions to interval timing. a) We examined cognitive behavior during a mouse-optimized interval timing task. In this task, mice are rewarded for switching from a short to a long nosepoke response port after approximately 6 seconds; switching response ports (in green) is an explicit time-based decision, as in other interval timing tasks. b) During surgery, we injected viruses, implanted fiber optics, and implanted electrode or optrode arrays. Then we trained mice to perform the interval timing task; and finally, we performed pharmacological, optogenetic, and neuronal ensemble recording experiments. We manipulated striatal pathways involving c) D2-MSNs (red pseudocolor of Cre-dependent yellow-fluorescent protein (YFP) in a D2-Cre mouse) or d) D1-MSNs (blue pseudocolor of Cre-dependent YFP in a D1-Cre mouse) which project from the striatum (Str) to downstream basal ganglia structures such as the globus pallidus external (GPe) and internal (GPi) segments, as well as the substantia nigra pars reticulata (SNr). Panels a and b were created with BioRender.com.

117 ***Disrupting D2-MSNs or D1-MSNs delay interval timing.***

118 In 10 mice (5 female), we found that systemic drug injections targeting D2-dopamine
119 receptors (D2 blockade; sulpiride 12.5 mg/kg) reliably slowed timing by increasing switch times
120 relative to saline sessions (median (IQR); saline: 8.9 (8.4-9.8); D2 blockade: 10.1 (9.4-10.8); p =
121 0.002, Cohen's d = 1.0; Fig 2a–b)[37,38]. Because systemic D2 blockade can be non-specific, we
122 leveraged cell-type-specific optogenetics. We virally expressed the inhibitory opsin
123 halorhodopsin (Halo) in 10 D2-Cre mice (5 female) to inhibit dorsomedial striatal D2-MSNs
124 (Fig 1c; Fig S1). As with D2 blockade, we found that D2-MSN inhibition reliably increased
125 switch times (Fig 2c-d; Laser Off: 8.6 seconds (8.3–9.3); Laser On: 10.2 seconds (9.4–10.2);
126 signed rank p = 0.002, Cohen's d = 1.7; no effect in no-opsin controls; Fig S2). These data are
127 consistent with past work demonstrating that dorsomedial D2-MSNs reliably contribute to
128 timing[36–38].

129 Next, we investigated D1-MSNs[3,4,42]. In the same 10 mice as above with D2 blockade,
130 we found that systemic drugs blocking D1-dopamine receptors (D1 blockade; SCH23390 0.05
131 mg/kg) slowed interval timing by increasing switch times (saline: 9.7 (9.0-9.9); D1 blockade:
132 10.1 (9.3-11.4); p = 0.04, Cohen d = 0.7; Fig 2e-f). Furthermore, in 6 D1-Cre mice (3 female),
133 optogenetic inhibition of dorsomedial striatal D1-MSNs increased switch times (Fig 2g-h; Laser
134 Off: 8.7 seconds (8.0–9.1); Laser On: 10.5 seconds (9.6–11.1); signed rank p = 0.03, Cohen's d =
135 1.4; no effect in no-opsin controls; Fig S1-2). These data suggest that D1-MSNs and D2-MSNs
136 play similar roles in interval timing because disrupting either MSN type slowed timing by
137 increasing switch times[38,39].

138

139

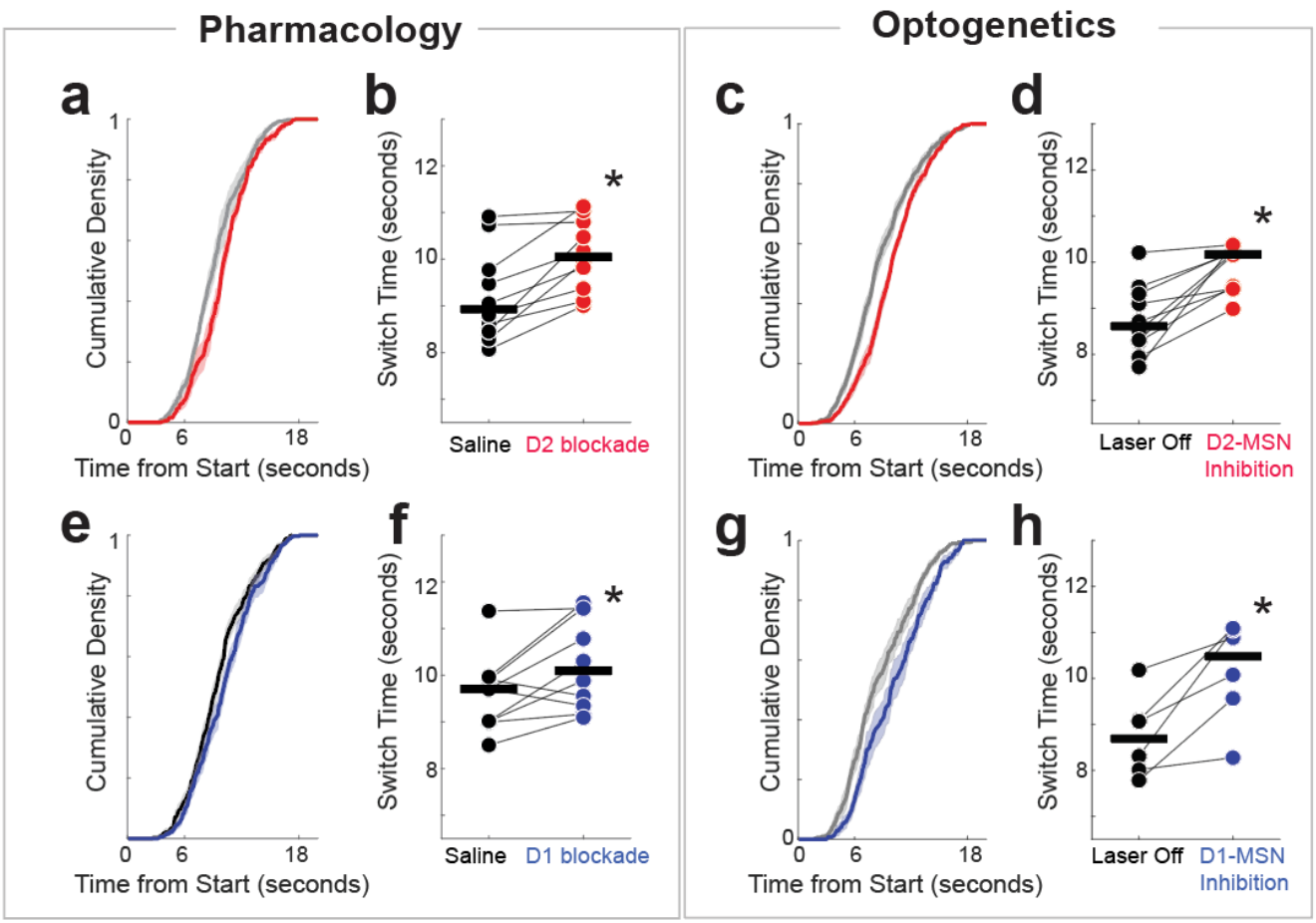

Figure 2: Disrupting D2- or D1-MSNs increases switch times. Pharmacologically disrupting D2-dopamine receptors (red) with the D2 antagonist sulpiride slowed timing by shifting a**)** cumulative distribution functions to the right, and b) increased switch times; data from 10 wild-type (WT) mice. Optogenetic inhibition of D2-MSNs (red) also slowed timing by shifting c) cumulative distributions to the right, and d) increased switch times; data from 10 D2-Cre mice expressing halorhodopsin (Halo). Similarly, pharmacologically disrupting D1-dopamine receptors (blue) with SCH23390 slowed timing and shifted e) cumulative distribution functions to the right, and f) increased switch times; data from the same 10 WT mice as in a-b. In addition, optogenetic inhibition of D1-MSNs (blue) slowed timing and shifted g) cumulative distributions to the right and h) increased switch times; data from 6 D1-Cre mice expressing Halo. In c, d, f, and h, connected points represent the mean switch time from each animal in each session, and horizontal black lines represent group medians. *p = < 0.05, signed rank test.

141 ***Disrupting D2-MSNs or D1-MSNs does not affect task-specific movement.***

142 MSNs can influence motor control, particularly in the dorsolateral striatum[2,3,5,8].
143 Critically, we found no evidence that inhibiting D2-MSNs in the dorsomedial striatum changed
144 task-specific movements such as response duration (signed rank $p = 0.63$; Fig 3a-b) or switch
145 traversal time between the short and long response ports (signed rank $p = 0.49$; Fig 3c).
146 Similarly, we found no evidence that D1-MSN inhibition changed response duration (signed
147 rank $p = 0.31$; Fig d-e) or traversal time (signed rank $p = 0.22$; Fig 3f). Furthermore, disrupting
148 D2-MSNs or D1-MSNs did not change switch time standard deviations or the number of rewards
149 (Fig S3). These results indicate that disrupting dorsomedial striatal D2-MSNs and D1-MSNs
150 specifically slowed interval timing without consistently changing task-specific movement.

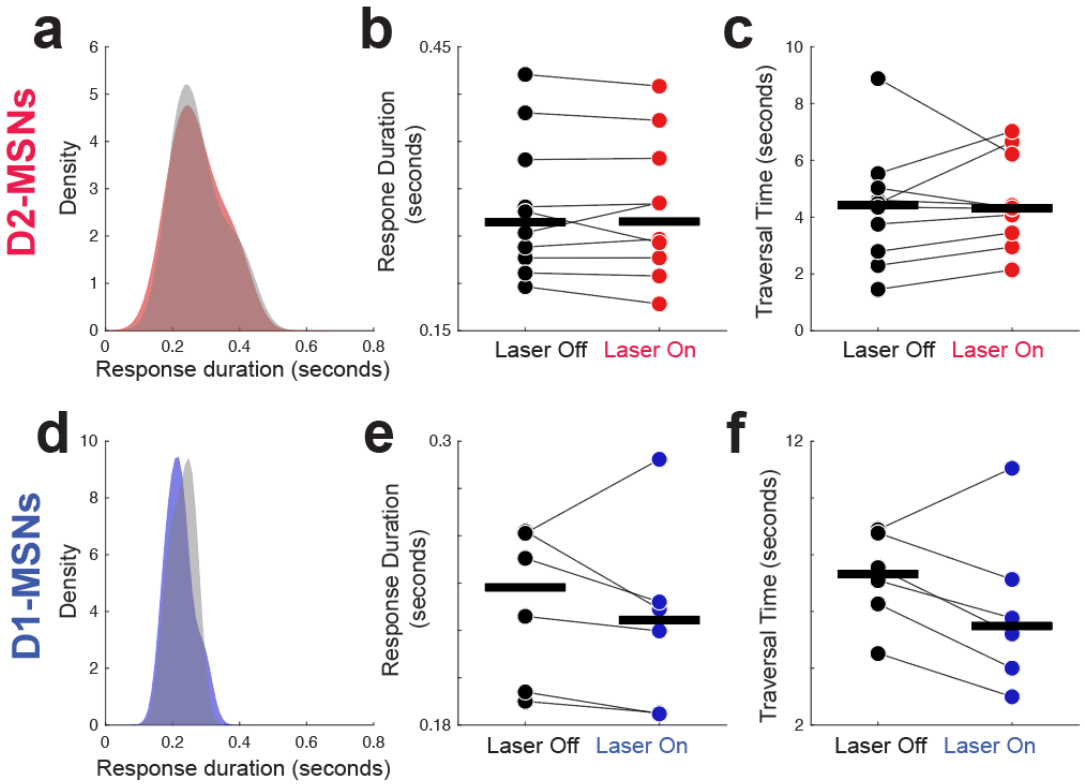

Figure 3: Optogenetically inhibiting D2-MSNs or D1-MSNs does not affect task-specific motor control. During interval timing there was no effect of optogenetic inhibition (red) of dorsomedial striatal D2-MSNs on a-b) switch response duration (time of response port entry to exit) or c) the switch traversal time between the short- and long-response ports. There was also no effect of optogenetic inhibition (blue) of dorsomedial striatal D1-MSNs on switch response duration (d-e) or f) or switch traversal time. Data from the same 10 D2-Cre mice and 6 D1-Cre mice, as in Figure 2. Horizontal black lines in b, c, e, and f represent group medians.

151 ***D2 blockade and D1 blockade degrade MSN temporal encoding.***

152 MSNs strongly encode time[28–31,34,43], but it is unknown how striatal ensembles are
153 affected by drugs disrupting D2- or D1-dopamine receptors[9]. We investigated this idea by
154 recording from dorsomedial striatal MSN ensembles in 11 mice during sessions with saline, D2
155 blockade with sulpiride, or D1 blockade with SCH23390 (Fig 4a; Figs S4 and S5). We analyzed
156 MSN ensembles in sessions with saline (158 neurons), D2 blockade (167 neurons), or D1
157 blockade (144 neurons; Fig 4b-c).

158 We quantified striatal MSN temporal encoding via a naïve Bayesian classifier that
159 generates trial-by-trial predictions of time from MSN ensemble firing rates (Fig 4d)[28,34].
160 Inspection of prediction matrices from saline sessions revealed strong temporal predictions early
161 in the interval (0–6 seconds; $R^2 = 0.91$ (0.83–0.94)) with weaker predictions later in the interval
162 (6–12 seconds: $R^2 = 0.55$ (0.33–0.70); rank sum $p = 0.00002$ vs 0–6 seconds, Cohen $d = 2.1$; 12–
163 18 seconds: $R^2 = 0.16$ (0.08–0.64); rank sum $p = 0.00005$ vs 0–6 seconds, Cohen $d = 2.3$; all
164 sessions were considered statistically independent; Fig 4e). Remarkably, we found that temporal
165 encoding early in the interval (0–6 seconds) was degraded with either D2 blockade ($R^2 = 0.69$
166 (0.59–0.84); rank sum $p = 0.0003$ vs saline, Cohen $d = 1.4$) or D1 blockade ($R^2 = 0.70$ (0.47–
167 0.87); rank sum $p = 0.006$ vs saline, Cohen $d = 1.2$; Fig 4e). Later in the interval (6–12 and 12-18
168 seconds), there were no significant differences between saline sessions and D2 blockade or D1
169 blockade (Fig 4e). These data demonstrate that disrupting either D2-MSNs or D1-MSNs
170 degrades MSN temporal encoding.

171

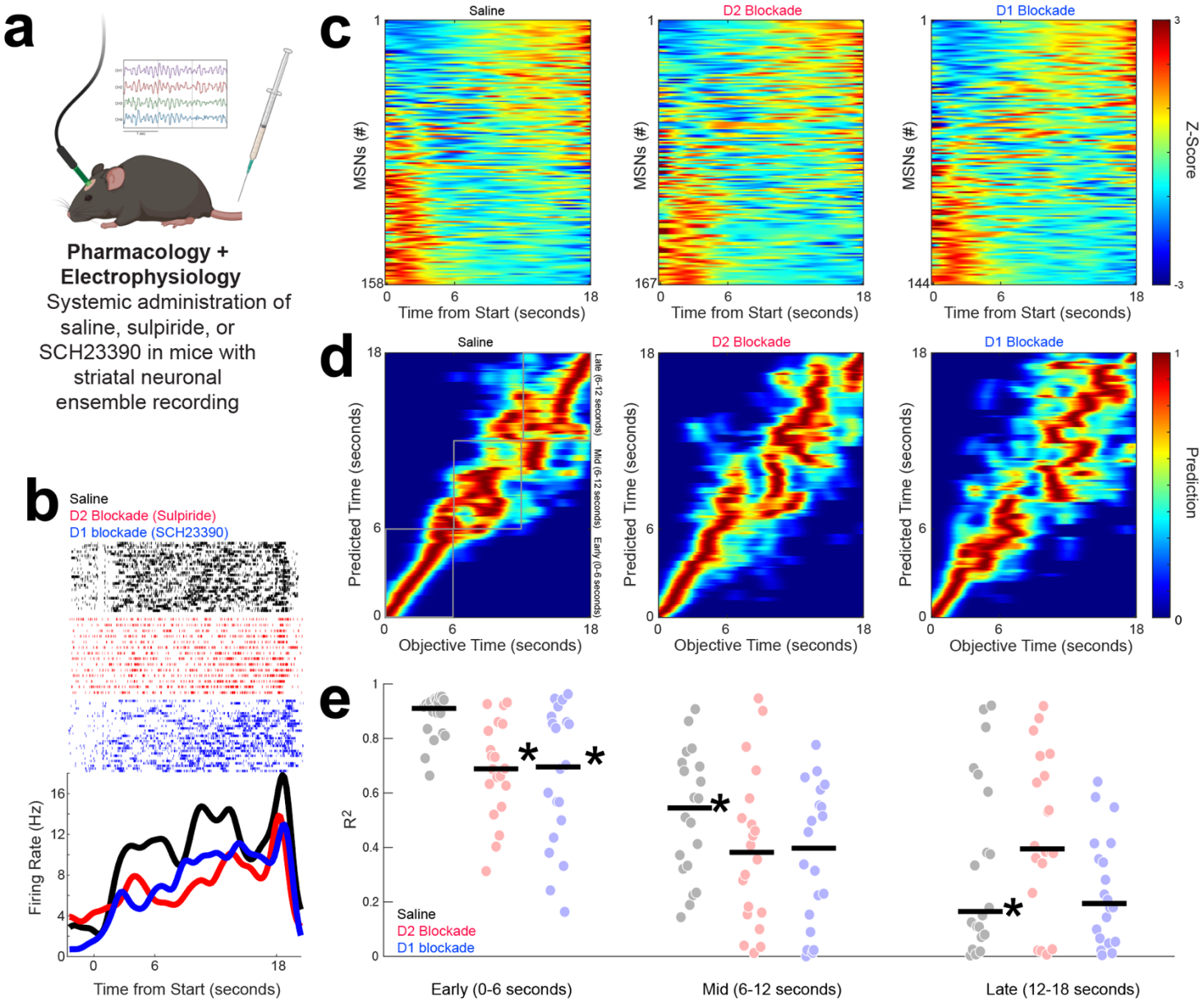

Figure 4: D2 and D1 blockade degrade temporal encoding. a) We recorded dorsomedial striatal medium spiny neuron (MSN) ensembles during interval timing in sessions with saline, D2 blockade with sulpiride, or D1 blockade with SCH23390. Made with BioRender.com. b) Peri-event raster from a single MSN in sessions with saline (black), D2-dopamine blockade (red), or D1-dopamine blockade (blue). D2 blockade or D1 blockade changed this MSN's temporal dynamics. c) Neuronal ensemble recording from the same 11 animals with saline, D2 blockade, or D1 blockade; each row represents a peri-event time histogram. Colors indicate z-scored firing rate. d) We used naïve Bayesian classifiers to decode time from MSN ensembles (see Methods and Materials). Each color represents the temporal prediction across 20 trials and red represents stronger predictions. e) Temporal encoding was strong early in the interval, and D2 or D1 blockade degraded classification accuracy. Temporal encoding was decreased later in the interval. Each point represents the R^2 for each trial of behavior for MSN ensembles from 11 mice. * $p < 0.05$ vs saline from 0-6 seconds. Horizontal black lines in (e) represent group medians.

We harnessed principal component analyses (PCA) to identify patterns of MSN ensemble activity across the interval[28,34,44]. We focused our analyses early in the interval (0–6 seconds) because temporal encoding during this epoch was powerfully affected by D2 and D1 blockade (Fig 4e), and this window captured MSN population dynamics before most switch responses (Fig 5a). Population analyses were performed by constructing principal components (PC) from z-scored peri-event time histograms of firing rate on switch trials. Saline, D2 blockade, and D1 blockade sessions were considered independently (see Fig S6-7 for analyses of neurons across sessions). PCs were computed from all sessions simultaneously. Examination of the individual components revealed that the first component (PC1), which explained 55% of neuronal variance, exhibited "time-dependent ramping", or monotonic changes in firing rate, over the first 6 seconds of the interval. The second component (PC2) explained 31% of the variance (Fig 5b). Interestingly, PC1 was decreased with both D2 blockade (D2 blockade (0.73 (-6.38–5.08) vs saline: 3.68 (-4.04–5.78); rank sum $p = 0.03$ vs saline, Cohen's $d = 0.2$) and in sessions with D1 blockade (0.71 (-6.69– 5.19); rank sum $p = 0.01$ vs saline, Cohen's $d = 0.3$; Fig 5c). Few reliable differences were found in PC2 or higher components (Fig 5d). Together, these findings further suggest that D2 and D1 blockade have similar effects on MSN population dynamics.

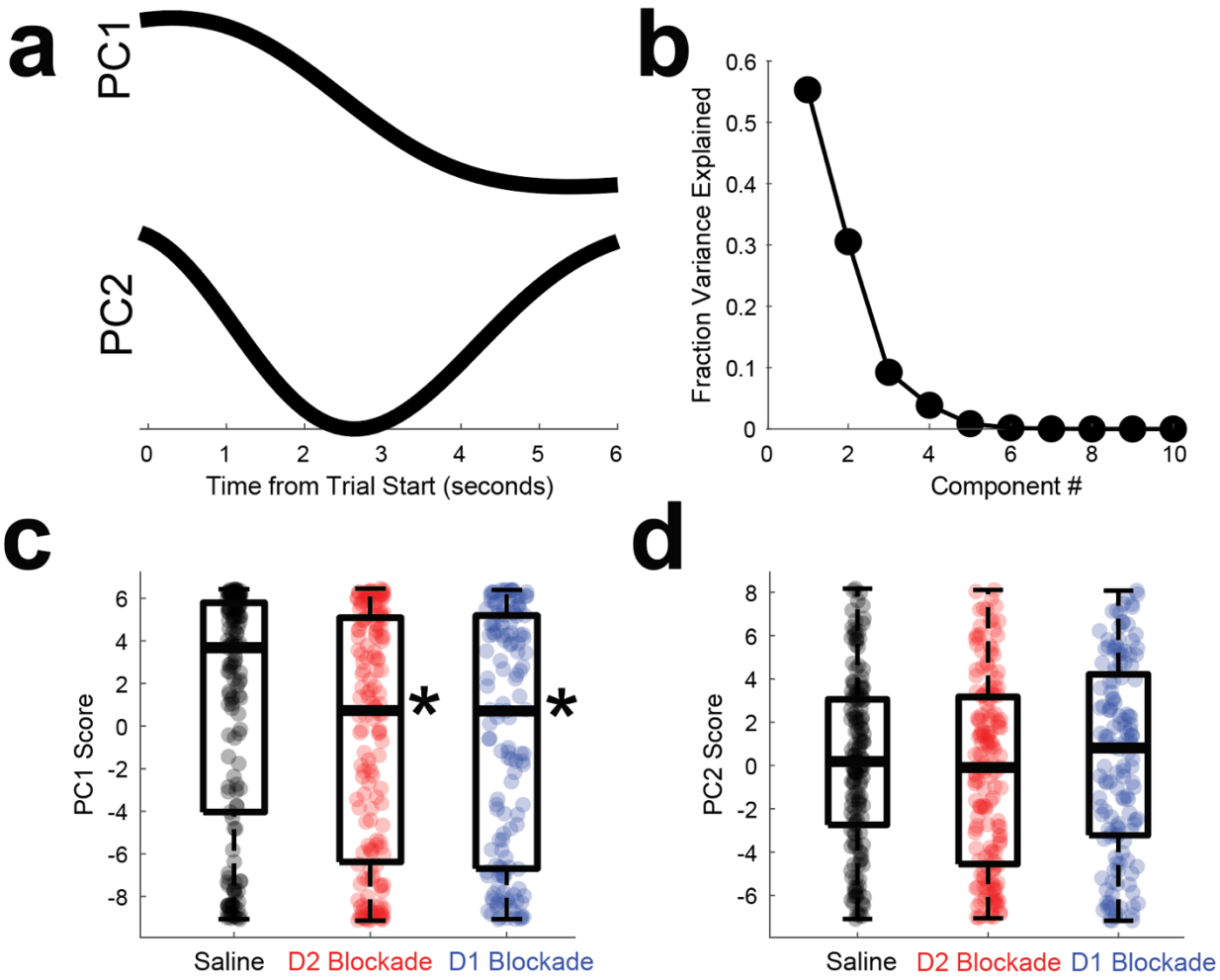

Figure 5: D2 and D1 blockade disrupt prominent patterns of MSN population activity. a) We leveraged principal component analysis to identify patterns of activity among MSN ensembles. The first principal component (PC1) exhibited time-dependent ramping. b) PC1 explained 55% of population variance among MSN ensembles; the second principal component (PC2) explained 31%; higher components explained <10% and were not analyzed. c) PC1 scores were significantly different with D2 or D1 blockade, but d) PC2 scores were not. MSN ensembles from 11 mice. *$p < 0.05$; data from the same mice as in Figure 4.

190

191 ***D2-MSNs and D1-MSNs have opposite patterns of temporal encoding.***

192 Striatal neuronal populations are composed of MSNs expressing D2-dopamine or D1-
193 dopamine receptors. We studied dorsomedial D2-MSN vs D1-MSN activity with optogenetic
194 tagging in transgenic mice in which we could identify each cell class[45–48]. To tag MSNs, we
195 expressed channelrhodopsin (ChR2) in 4 D2-Cre mice (2 female) and 5 D1-Cre mice (2 female)
196 and identified D2-MSNs or D1-MSNs neurons by their response to 5 millisecond pulses of 473-
197 nm light (Fig S8). We tagged 32 D2-MSNs and 41 D1-MSNs (Fig 6a–d). Strikingly, D2-MSN
198 populations tended to ramp up while D1-MSN populations tended to ramp down (Fig 6c–e).

199 We used PCA to analyze MSN populations calculated from peri-event matrices from D1-
200 MSNs and D2-MSNs[47,49]. PCA identified time-dependent ramping activity as PC1 (Fig 6f), a key
201 temporal signal that explained 56% of variance among tagged neurons[50]. We found that D2-
202 MSNs and D1-MSNs had opposite patterns of activity with negative PC1 scores for D2-MSNs
203 and positive PC1 scores for D1–MSNs (Fig 6f–g; PC1 for D2-MSNs: -5.05 (-6.40–3.35); PC1
204 for D1-MSNs: 4.21 (-4.52–6.92); rank sum $p = 0.003$, Cohen's $d = 0.7$). These data imply that
205 D2-MSN populations tended to ramp up, while D1-MSN populations tended to ramp down
206 opposite that of D2-MSNs.

207 To explore these dynamics in detail, we calculated the linear slope of D2-MSN and D1-
208 MSN activity using generalized linear modeling (GLM) of trial-by-trial firing rate[51,52]. GLM
209 analysis revealed that D2-MSNs tended to have a positive linear slope of firing rate vs time in
210 the interval (0.02 spikes/second (-0.07–0.21)), also implying that D2-MSNs tended to ramp up
211 (Fig 6h; compare with PCA in Fig 6f-g) compared to D1-MSNs, which tended to ramp down (-
212 0.14 spikes/second (-0.35–0.01); rank sum $p = 0.002$, Cohen's $d = 0.7$). Differences between D2-
213 MSNs and D1-MSNs were consistent over the entire 0–18 second interval (Fig S9). Together,

214 this line of evidence indicates that D2-MSNs and D1-MSNs have opposing patterns of neuronal

215 firing over the temporal interval defined by PC1 and by GLM-defined linear slope.

216

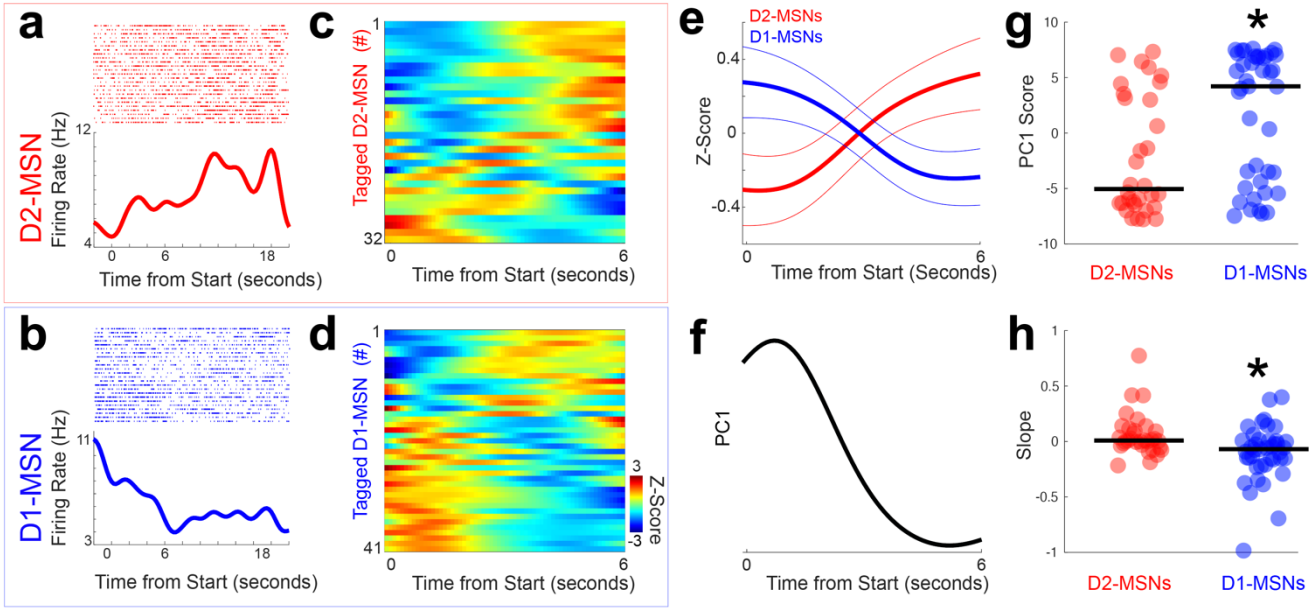

Figure 6: D2-MSNs and D1-MSNs have opposite dynamics. We used optogenetic tagging to record from D2-MSNs and D1-MSNs (Figure S8). Peri-event raster a) from a D2-MSN and b) from a D1-MSN. Histograms derived from the firing rate across trials. c) Peri-event time histograms from D2-MSNs and d) from D1-MSNs. e) D2-MSNs (red) tended to ramp up, whereas D1-MSNs (blue) tended to ramp down. f) Principal component analysis revealed that the first component (PC1) exhibited time-dependent ramping. This component explained ~56% of variance across tagged MSN ensembles. g) Differences between D2-MSNs (red) and D1-MSNs (blue) were captured in PC1, which captures time-dependent ramping. h) These differences were also apparent in the linear slope of firing rate vs time in the interval, with D1-MSNs (blue) having a more negative slope than D2-MSNs (red). Data from 32 tagged D2-MSNs in 4 D2-Cre mice and 41 tagged D1-MSNs in 5 D1-Cre mice. In g and h, each point represents data from each tagged MSN, and horizontal black lines represent group medians. * $p < 0.05$.

Drift-diffusion models capture complementary D2-MSN and D1-MSN dynamics.

Our data demonstrate that D2-MSNs and D1-MSNs have similar effects on interval timing behavior and MSN temporal encoding but opposite activity patterns. We turned to computational modeling to reconcile similar behavioral/encoding effects despite opposing dynamics. Past computational models of interval timing have relied on drift-diffusion dynamics with a positive slope that accumulates evidence over time[53–56]. However, our optogenetic tagging experiments indicated that D2-MSNs tend to ramp up while D1-MSNs tend to ramp down. To demonstrate how these MSNs might complement each other to control movement in time, we constructed a four-parameter drift-diffusion model, where x represents the neuronal firing rate, t represents time measured in seconds, and dx and dt mean "change" in x and t respectively (equivalent to the derivative dx/dt):

$$dx = (F - x)Ddt + \sigma d\xi(t) \qquad \text{(Equation 1)}$$

$$x(0) = b \qquad \text{(Equation 2)}$$

The model has four independent parameters F, D, σ, and b (described below) and a threshold value T defined by

$$T = T(F, b) = \left(1 - \frac{1}{4}b\right)F + \frac{1}{4}b(1 - F). \qquad \text{(Equation 3)}$$

The firing rate is set initially at baseline b (see Equation 2), then driven by input F akin to the dendritic current induced by the overlap of cortico-striatal postsynaptic potentials. With each unit of time *dt*, we suppose there is corticostriatal input that provides incremental input proportional to the activity itself, $(F - x)D$, to reach a decision. D is *the drift rate* for the event sequence, which with noise $\xi(t)$ (of zero mean and strength σ) leads to fluctuating accumulation and eventually crosses a threshold T (see Equation 3; Fig 7A–B). The time t^* it takes the firing rate to reach the threshold, $x(t^*) = T$, is the *switch time*.

We report that models like Equations 1–3 generate switch times consistent with gamma-like response statistics observed in the behavioral data (one-sample Kolmogorov-Smirnov test for goodness of fit: control $p = 0.27$, inhibition $p = 0.11$; Fig S10). Surprisingly, the same model strongly and parsimoniously fit four conditions: 1) interval timing behavior for D2-Cre mice (data from Fig 2d-f; Laser Off trials $R^2 = 0.63$ vs model; Fig 7C, in black); 2) interval timing behavior for D1-Cre mice (data from Fig 2j-l; trials with Laser Off trials $R^2 = 0.64$ vs model; Fig 7d, in black); 3) interval timing behavioral data with D2-MSN optogenetic inhibition ($R^2 = 0.55$; Fig 7c, in red); and 4) interval timing behavior with D1-MSN optogenetic inhibition ($R^2 = 0.57$; Fig 7d, in blue). In Figs 7 and S10, the parameters were chosen as follows. 1) D2: $F = 1$; $b = 0.52$ (so $T = 0.87$); $D = 0.14, \sigma = 0.05$ for control; and $D = 0.14, \sigma = 0.04$ for inhibition. 2) D1: $F = 0$; $b = 0.48$ (so $T = 0.13$); $D = 0.14, \sigma = 0.05$ for control; and $D = 0.12$, $\sigma = 0.04$ for inhibition. These data refine prior drift-diffusion models with dynamics inspired by electrophysiology and, with relatively few parameters, can explain interval timing behavior as well as disruptions in D2- and D1-MSNs[54,55]. This model describes how D2-MSNs and D1-MSNs make complementary cognitive contributions to the temporal control of action.

In summary, we demonstrated that disrupting either D2-MSNs or D1-MSNs slowed interval timing and degraded temporal encoding. Surprisingly, we found that D2-MSNs and D1-MSNs have opposite dynamics during interval timing. Finally, we used these data to construct a four-parameter drift-diffusion model of interval timing that explains baseline behavior as well as D2/D1 perturbations. This line of work provides novel insight into cognitive computations by the striatum.

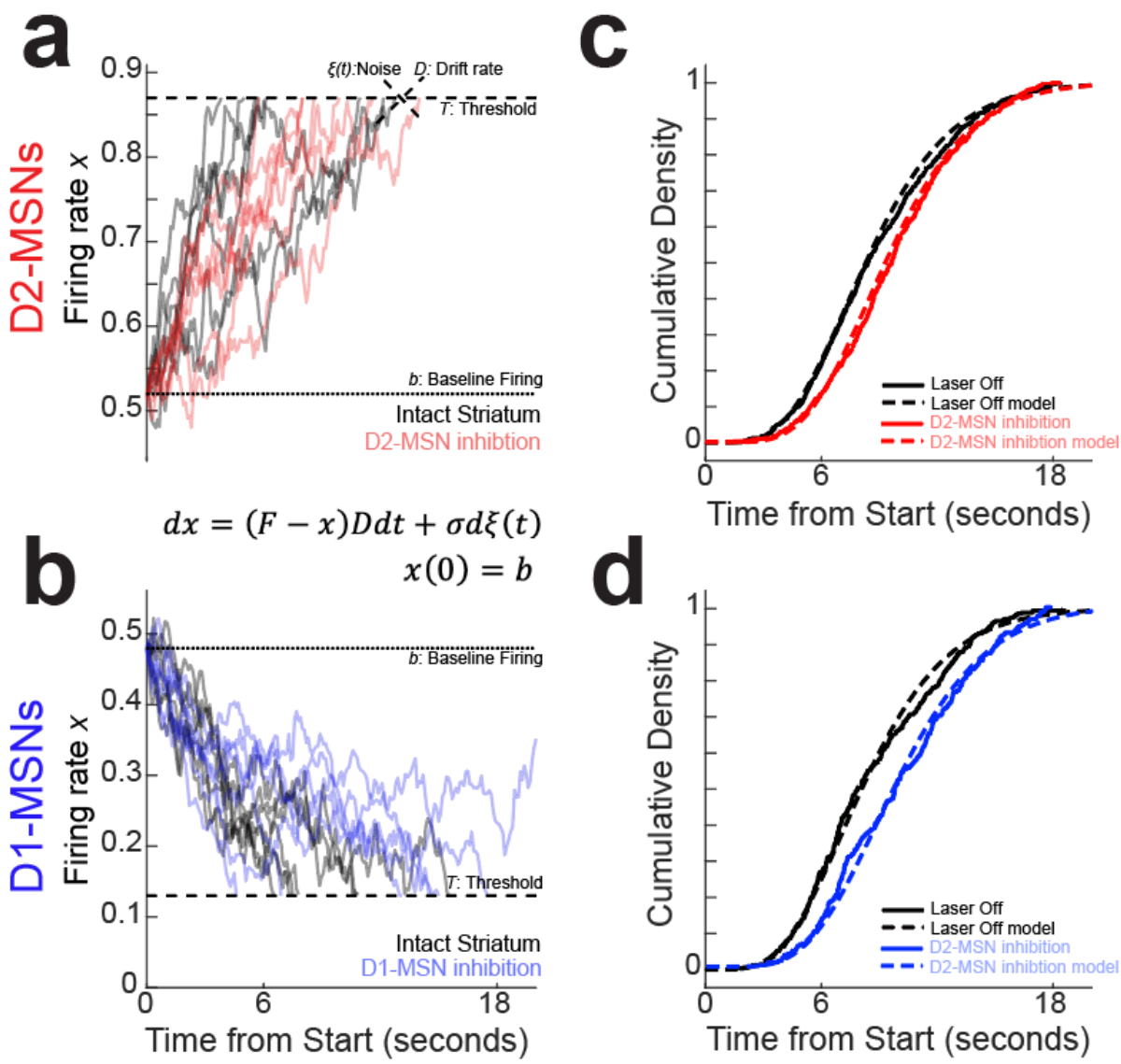

Figure 7: Four-parameter drift-diffusion computational model of complementary interval timing dynamics. Drift-diffusion computational model of striatal activity during interval timing. a) We modeled interval timing with a low parameter diffusion process with a drift rate *D*, noise $\xi(t)$, a baseline firing rate *b* drift toward a threshold *T* indicated by dotted lines. With D2-MSNs disrupted, this drift process decreases in slope and takes longer to reach the threshold. b) The same model also accounted for D1-MSNs that had an opposite drift slope. Fit between empirical behavioral data (solid lines) and computational models (dashed lines) for both c) D2-Cre mice and d) D1-Cre mice expressing halorhodopsin. Data from inhibition trials are in red (D2-MSNs) or blue (D1-MSNs); data from trials with the Laser Off are in black. Threshold *T* depends on *b* and target firing *F*. This four-parameter model explained timing behavior as well as D2-MSN and D1-MSN disruptions.

DISCUSSION

We explored how striatal MSN ensembles encode an elementary cognitive process, interval timing. We found that pharmacologically or optogenetically disrupting striatal D2-MSNs or D1-MSNs slowed timing, increasing an animal's self-reported estimates of time without affecting task-specific motor behavior. Furthermore, D2 blockade or D1 blockade degraded MSN temporal encoding. To our surprise, optogenetic tagging revealed that D2-MSNs and D1-MSNs had opposing patterns of activity with D2-MSNs ramping up over the interval and D1-MSNs ramping down. We reconciled these opposing dynamics and similar behavioral and temporal encoding effects of D2-MSN and D1-MSN perturbations with a four-parameter drift-diffusion model. Taken together, these data provide new insight into how opposing patterns of striatal MSN activity might influence behavior in similar ways, suggesting that they make complementary contributions to elementary cognitive operations.

Striatal MSNs are critical for temporal control of action[29,57]. Three broad models have been proposed for how striatal MSN ensembles represent time: 1) the striatal beat frequency model, in which MSNs encode temporal information based on neuronal synchrony[58]; 2) the distributed coding model, in which time is represented by the state of the network[29,59]; and 3) the drift-diffusion model, in which neuronal activity monotonically drifts toward a threshold after which responses are initiated[30,54,60]. While our data do not formally resolve these possibilities, our results suggest that D2-MSN and D1-MSN activity exhibit opposing firing rate dynamics with linear changes in firing rates over the interval. Furthermore, we find that low-parameter drift-diffusion models account for interval timing behavior with both intact and disrupted striatal D2- and D1-MSNs. While it is possible that other models might capture interval timing behavior

286 and account for MSN neuronal activity, our model does so parsimoniously with relatively few
287 parameters.

288 D2-MSNs and D1-MSNs have been proposed to play complementary roles in movement.
289 For instance, stimulating D1-MSNs facilitates movement, whereas stimulating D2-MSNs
290 impairs movement[5]. Both populations have been shown to have complementary patterns of
291 activity during movements[3,4], with MSNs firing at different phases of action initiation and
292 selection. Further dissection of action selection programs reveals that opposing patterns of
293 activation among D2-MSNs and D1-MSNs suppress and guide actions, respectively, in the
294 dorsolateral striatum[2]. Our data extend these findings to interval timing, which is an elementary
295 cognitive process requiring working memory for temporal rules as well as attention to the
296 passage of time. A particular advantage of interval timing is that it captures a cognitive behavior
297 within a single dimension — time. When projected along the time dimension, it is remarkable
298 that D2-MSNs and D1-MSNs have opposing patterns of activity. Our behavioral results and
299 computational modeling suggest that disrupting either D2-MSNs or D1-MSNs increased self-
300 reported estimates of time, indicating that disrupting either D2-MSN or D1-MSN activity
301 degrades temporal encoding. Our recording experiments do not identify where a possible
302 response threshold T is instantiated, but downstream basal ganglia structures may have a key role
303 in setting response thresholds[61].

304 Since interval timing is reliably disrupted in human diseases of the striatum such as
305 Huntington's disease, Parkinson's disease, and schizophrenia[16,21,62,63], our results have relevance
306 to human disease. Furthermore, because many therapeutics targeting dopamine receptors are
307 used clinically, our results may help illuminate how dopaminergic drugs affect cognitive
308 function and dysfunction[64,65]. Finally, D2-MSNs and D1-MSNs define indirect and direct

309 pathways, which are targeted by deep brain stimulation for neurological and psychiatric
310 disease[66,67].

311 Our approach has several limitations. First, systemic drug injections will block D2- and
312 D1-receptors in many different brain regions, including the frontal cortex, which we have shown
313 to be involved in interval timing[47]. D2 blockade or D1 blockade may have complex effects,
314 including corticostriatal or network effects that contribute to changes in D2-MSN or D1-MSN
315 ensemble activity[9]. Second, optogenetic tagging is low-yield, and it is possible that recording
316 more of these neurons would afford greater opportunity to identify alternative coding schemes,
317 such as neuronal synchrony[58]. Third, the striatum includes diverse cell types that may play a key
318 role[68]. Fourth, MSNs can laterally inhibit each other, which may profoundly affect striatal
319 function[69]. Regardless, we show that cell-type-specific disruption of D2-MSNs and D1-MSNs
320 both slow timing, implying that these cell types play a key role in interval timing, and our
321 optogenetic tagging experiments describe their activity at high temporal resolution. Future
322 experiments may record from non-MSN striatal cell types, including fast-spiking interneurons
323 that shape basal ganglia output[70]. Fifth, there may be key anatomic differences between dorsal
324 striatal regions that we did not capture[71]. Finally, we did not deliver stimulation to the striatum,
325 because our pilot experiments triggered movement artifacts or task-specific dyskinesias[72,73].
326 Future stimulation approaches carefully titrated to striatal physiology may influence interval
327 timing without affecting movement[48].

328 In summary, we examined the role of dorsomedial striatal D2-MSNs and D1-MSNs
329 during an elementary cognitive behavior, interval timing. We found that disrupting either D2-
330 MSNs or D1-MSNs impaired estimates of time and degraded temporal encoding by striatal
331 ensembles. Optogenetic tagging revealed that D2-MSNs and D1-MSNs exhibited opposite,

complementary patterns of neuronal activity. Finally, these patterns could be captured by computational drift-diffusion models. Collectively, our data provide insight into how the striatum encodes cognitive information, which could be highly relevant for human diseases that disrupt the striatum and for next-generation neuromodulation that targets the basal ganglia to avoid cognitive side effects or to treat cognitive dysfunction.

338 **Methods and Materials**

339 ***Rodents.*** All procedures were approved by the Institutional Animal Care and Use Committee
340 (IACUC) at the University of Iowa, and all experimental methods were performed in accordance
341 with applicable guidelines and regulations (Protocol #0062039). We used three mouse lines. For
342 behavioral pharmacology experiments, we used C57BL/6J mice (10 mice (5 female); The
343 Jackson Laboratory, Bar Harbor, ME). For cell-type-specific optogenetics and electrophysiology,
344 we used either *Drd2-cre+* mice derived from Gensat strain ER44 (10 mice (5 female) for
345 optogenetic inhibition; 5 mice (2 female) for optogenetic controls; 4 mice (2 female) for
346 tagging)[74] or *Drd1-cre+* mice derived from Gensat strain EY262 (6 mice (3 female) for
347 optogenetic inhibition; 5 mice (3 female) optogenetic controls; 5 mice (2 female) for tagging).
348 For combined behavioral pharmacology and electrophysiology, we used 11 mice (4 C57BL/6J (2
349 female), 5 *Drd2-cre+* mice (2 female), and 2 *Drd1-cre+* mice (0 female)).

350 ***Interval timing switch task.*** We used a mouse-optimized interval timing task described in detail
351 previously[33,34,37,40,75,76]. Briefly, mice were trained in sound-attenuating operant chambers, with
352 two nosepoke response ports flanking either side of a food hopper on the front wall, and a third
353 nosepoke response port located at the center of the back wall. The chamber was positioned below
354 an 8-kHz, 72-dB speaker (Fig 1A; MedAssociates, St. Albans, VT). Mice were 85% food
355 restricted and motivated with 20 mg sucrose pellets (Bio-Serv, Flemington, NJ). Mice were
356 initially trained to receive sucrose rewards during fixed ratio nosepoke response trials. After
357 shaping, mice were trained in the "switch" interval timing task[33]. Mice initiated trials at the back
358 response port, after which a tone and nosepoke lights were illuminated simultaneously. Response
359 port entry and exit were captured by infrared beams. On short trials (50% of randomly selected

360 trials), mice were rewarded after 6 seconds for nosepoke responses at the designated short
361 response port (left or right). On long trials, mice were rewarded after 18 seconds for responding
362 first at the short response port and then switching responses to the long response port (left or
363 right). Critically, the decision to switch from the short to the long response port is a time-based
364 decision guided by internal estimates of time. All analyses were focused on long switch trials
365 when animals depart from the short response port. *Switch time* was defined as the moment an
366 animal exited the short response port prior to entering the long response port. We focused on the
367 switch time as a representation of temporal control of action. Switch *response duration* was
368 defined as the time between short response entry and exit for the switch responses only. Switch
369 *traversal time* was defined as the duration between short response port exit and long response
370 port entry.

371 ***Behavioral pharmacology procedures.*** C57BL/6J mice were injected intraperitoneally (IP) 20-
372 40 minutes before interval timing trials with either SCH23390 ($C_{17}H_{18}ClNO$; D1 antagonist),
373 sulpiride ($C_{15}H_{23}N_3O_4S$; D2 antagonist), or isotonic saline. The sulpiride dosage was 12.5 mg/kg,
374 0.01 mL/g, and the SCH23390 was administered at a dosage of 0.05 mg/kg, 0.01 mL/g.
375 Behavioral performance was compared with interval timing behavior on the prior day when
376 isotonic saline was injected IP.

377 ***Surgical and histological procedures.*** Surgical procedures were identical to methods described
378 previously[34]. Briefly, mice were anesthetized using inhaled 4% isoflurane and surgical levels of
379 anesthesia were maintained at 1-2% for the duration of the surgery. Craniotomies were drilled
380 above bilateral dorsal striatal anatomical targets, and optogenetic viruses (AAV5-DIO-
381 eNHPR2.0 (halorhodopsin), AAV5-DIO-ChR2(H134R)-mcherry (ChR), or AAV5-DIO-cherry

382 (control) from the University of North Carolina Viral Vector Core) were injected (0.5 uL of
383 virus, +0.9, ML +/-1.3, DV –2.7). Either fiber optics (Doric Lenses, Montreal Quebec; AP +0.9,
384 ML +/-1.3, DV –2.5) or 4 x 4 electrode or optrode arrays (AP +0.4, ML -1.4, DV -2.7 on the left
385 side only; Microprobes, Gaithersburg, MD) were positioned in the dorsal striatum. Holes were
386 drilled to insert skull screws to anchor headcap assemblies and/or ground electrode arrays and
387 then sealed with cyanoacrylate ("SloZap," Pacer Technologies, Rancho Cucamonga, CA),
388 accelerated by "ZipKicker" (Pacer Technologies) and methyl methacrylate (AM Systems, Port
389 Angeles, WA). Following postoperative recovery, mice were trained on the switch task and
390 acclimated to experimental procedures prior to undergoing experimental sessions.

391 ***Immunohistochemistry.*** Following completion of experiments, mice were transcardially
392 perfused with ice-cold 1x phosphate-buffered saline (PBS) and 4% paraformaldehyde (PFA)
393 after anesthesia using ketamine (100 mg/kg IP) and xylazine (10 mg/kg IP). Brains were then
394 fixed in solutions of 4% PFA and 30% sucrose prior to being cryosectioned on a freezing
395 microtome. Sections were stained for tyrosine hydroxylase with primary antibodies for >12
396 hours (rabbit anti-TH; Millipore MAB152; 1:1000) at 4° C. Sections were subsequently
397 visualized with Alexa Fluor fluorescent secondary antibodies (goat anti-rabbit IgG Alexa 519;
398 Thermo Fisher Scientific; 1:1,000) matched to host primary by incubating 2 hours at room
399 temperature. Histological reconstruction was completed using postmortem analysis of electrode
400 placement by slide-scanning microscopy on an Olympus VS120 microscope (Olympus, Center
401 Valley, PA; Fig S4).

402 ***Electrophysiology.*** Single-unit recordings were made using a multi-electrode recording system
403 (Open Ephys, Atlanta, GA), After the experiments, Plexon Offline Sorter (Plexon, Dallas, TX),

404 was used to remove artifacts. Spike activity was analyzed for all cells that fired at rates above 0.1
405 Hz. Principal component analysis (PCA) and waveform shape were used for spike sorting. Single
406 units were defined as those 1) having a consistent waveform shape, 2) being a separable cluster
407 in PCA space, and 3) having a consistent refractory period of at least 2 milliseconds in interspike
408 interval histograms. Putative MSNs were further separated from striatal fast-spiking interneurons
409 (FSIs) based on hierarchical clustering of the waveform peak-to-trough ratio and the half-peak
410 width (*fitgmdist* and *cluster.m*; Fig S5)[77]. We calculated kernel density estimates of firing rates
411 across the interval (-4 seconds before trial start to 22 seconds after trial start) binned at 0.1
412 seconds, with a bandwidth of 1. We used PCA to identify data-driven patterns of z-scored
413 neuronal activity, as in our past work[28,34,78–80]. Average plots were shown with Gaussian
414 smoothing for plotting purposes only.

415 ***Optogenetics.*** We leveraged cell-type-specific optogenetics to manipulate D2-MSNs and D1-
416 MSNs in D2- or D1-cre mice. In animals injected with optogenetic viruses, optical stimulation
417 was delivered via bilateral patch cables for the entire trial duration of 18 seconds via 589-nm
418 laser light at 12 mW power on 50% of randomly assigned trials. For optogenetic tagging,
419 putative D1- and D2-MSNs were optically identified via 473-nm photostimulation. Units with
420 mean post-stimulation spike latencies of ≤5 milliseconds and a stimulated-to-unstimulated
421 waveform correlation ratio of >0.9 were classified as putative D2+ or D1+ neurons[81,82].

422 ***Modeling.*** We proposed a four-parameter drift-diffusion model (see Equations 1-3 in Results)
423 and used it to simulate response times compatible with mice behavioral data. The model was
424 implemented in MATLAB, starting from initial value b and with discrete computer simulation
425 steps $x_{new} = x_{old} + (F - x_{old})D\Delta t + \sigma\sqrt{\Delta t}N(0,1)$. Here $N(0,1)$ represents random values

426 generated from the standardized Gaussian distribution (mean = 0 and standard deviation = 1).
427 The integration timestep was taken $\Delta t = 0.1$ to be like the 0.1-second bin size used in the
428 analysis of firing rate data. For each numerical simulation, the "switch time" was defined as the
429 time t^* when variable x first reached the threshold value $T = F(1 - b/4) + (1 - F)b/4$. For
430 each condition, we ran 500 simulations of the model (up to 25 seconds per trial) and recorded the
431 switch times. Examples of firing rate x dynamics are shown in Figure 7a-b. We observed that the
432 distributions of interval timing response times could be fit by a gamma probability distribution
433 function $PDF(x) = \frac{\beta^\alpha}{\Gamma(\alpha)} x^{\alpha-1} e^{-\beta x}$ with shape α and rate β (see Fig S10). For D2-Cre data, we
434 found a good model fit: α = 6.03, β = 0.67 (empirical, Laser Off); α = 6.08, β = 0.69 (model,
435 Laser Off); α = 7.62, β = 0.78 (empirical, Inhibited); and α = 7.67, β = 0.79 (model, Inhibited);
436 Fig S10, left two columns. The fit for D1-Cre data was found at α = 5.87, β = 0.68 (empirical,
437 Laser Off); α = 5.89, β = 0.69 (model, Laser Off); α = 7.13, β = 0.70 (empirical, Inhibited); and
438 α = 7.31, β = 0.72 (model, Inhibited); Fig S10, right two columns.

439 ***Statistics.*** All data and statistical approaches were reviewed by the Biostatistics, Epidemiology,
440 and Research Design Core (BERD) at the Institute for Clinical and Translational Sciences
441 (ICTS) at the University of Iowa. All code and data are made available at
442 http://narayanan.lab.uiowa.edu/article/datasets. We used the median to measure central tendency
443 and the interquartile range to measure spread. We used Wilcoxon nonparametric signed rank or
444 rank-sum tests to compare behavior between experimental conditions and Cohen's *d* to calculate
445 effect size. When warranted (e.g., for paired comparisons of mean values, as in Fig 2b) we
446 applied the signed rank test instead. Analyses of putative single-unit activity and basic
447 physiological properties were carried out using custom routines for MATLAB[28,34,49,78].

Time-dependent ramping slope. To measure time-related ramping, we used generalized linear models (GLMs) at the individual neuron level in which the response variable was firing rate binned at 0.1 seconds and the predictor variable was time in the interval[83]. For each neuron, its time-related "ramping" slope was derived from the GLM fit of firing rate vs time in the interval, for all trials per neuron (see Fig 6). All models were run at a trial-by-trial level to avoid effects of trial averaging[51] as in our past work[28,34,78,84].

Bayesian classifier. As in our past work[28,78,79], we used a naïve Bayesian classifier to evaluate neuronal ensemble decoding from all neurons with at least 20 trials. To preclude edge effects that might bias classifier performance, we included data from 6 seconds prior to the trial start and 6 seconds after the end of the interval. We used leave-one-out cross-validation to predict an objective time from the firing rate within a trial. Classifier performance was quantified by computing the R^2 of objective time vs predicted time, only for bins during the interval (0-6, 6-12, and 12-18 seconds; see Fig 4). Classifier performance was compared using time-shuffled firing rates via a Wilcoxon signed rank test.

Data Availability

All raw data are available at http://narayanan.lab.uiowa.edu/article/datasets.

Code Availability

All code is available at http://narayanan.lab.uiowa.edu/article/datasets.

Acknowledgements

This work was funded by NIMH R01MH116043 to NSN

Author Contributions

RAB, MAW, and NN designed the experiments. RAB, CIAB, MAW, RV, and CJ performed all experiments and collected data. The data was analyzed by RAB, MAW, ASB, YK, RC, and NN. RC developed the computational model. AB, MAW, ASB, KS, RC, and NN wrote the manuscript, and all authors reviewed and revised the manuscript.

478 **Extended Data**

479

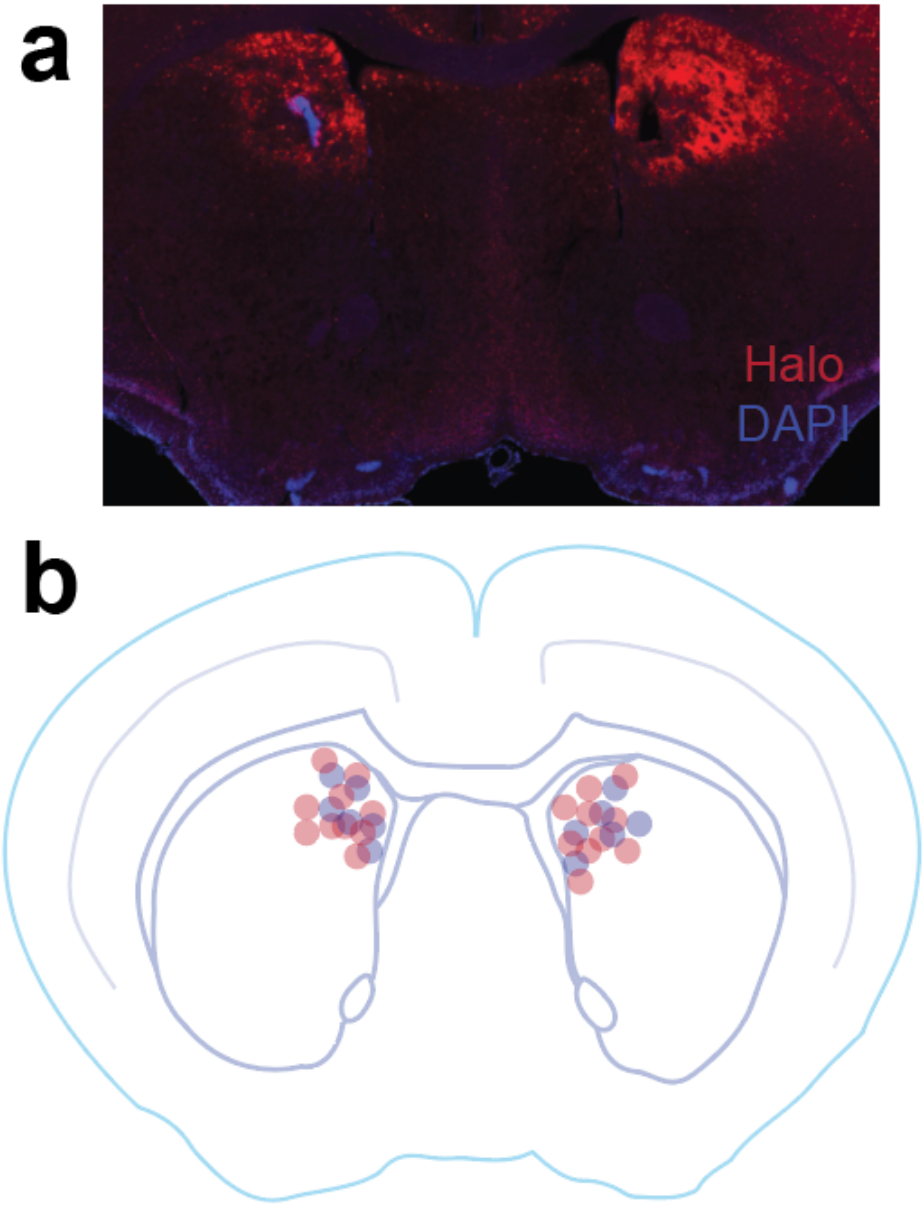

480

481

482 **Figure S1**: Fiber optic locations from a) an opsin-expressing mouse with mcherry-tagged

483 halorhodopsin and bilateral fiber optics, and b) across 10 D2-Cre mice (red) and 6 D1-cre mice

484 (blue) with fiber optics.

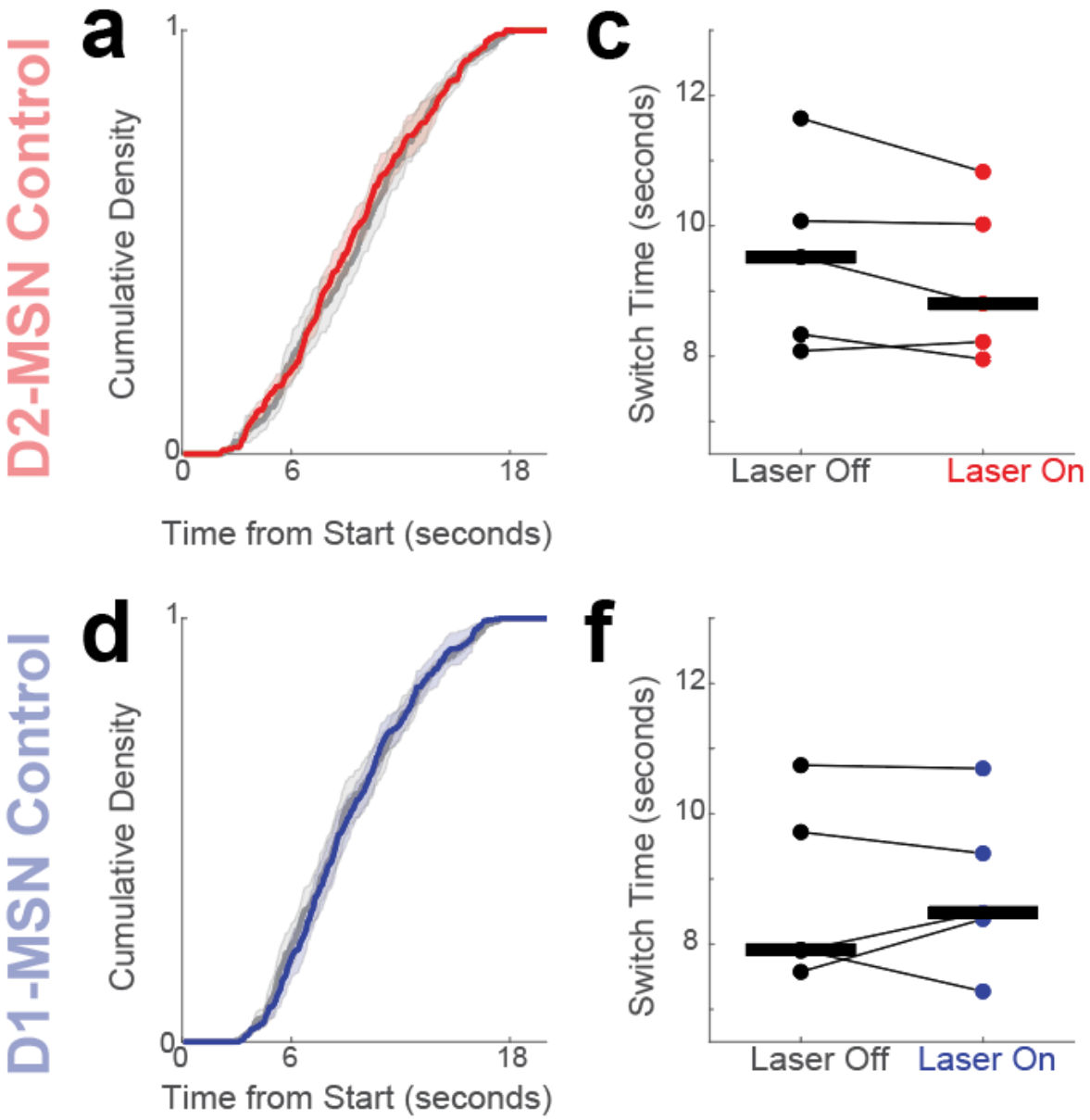

485

486

487 **Figure S2**: Experiments in D2-Cre mice injected with virus without opsins did not reliably affect

488 a) cumulative density functions (CDFs) or b) switch times (signed rank $p = 0.44$). Experiments in

489 D1-Cre mice expressing virus without opsins did not reliably affect c) CDFs or d) switch times

490 (signed rank $p = 0.81$).

491

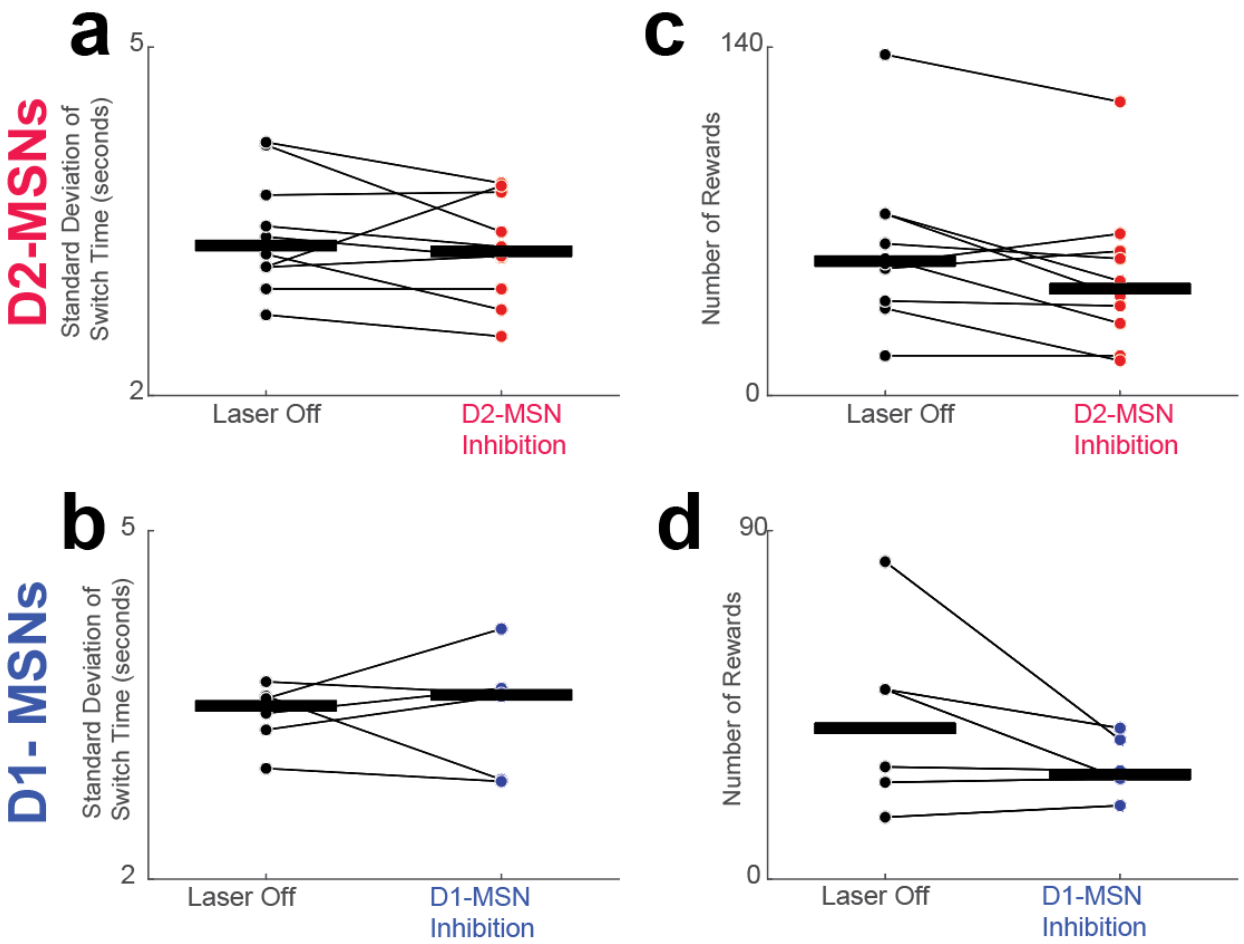

Figure S3: a) Standard deviation of interval timing performance for D2-MSN inhibition sessions (signed rank test, $p = 0.19$) and b) D1-MSN inhibition sessions ($p = 0.84$), and the number of total rewards for c) D2-MSN inhibition sessions ($p = 0.07$) and d) D1-MSN inhibition sessions ($p = 0.24$). Data from 10 D2-Cre mice and 6 D1-Cre mice as in Figs 2 and 3.

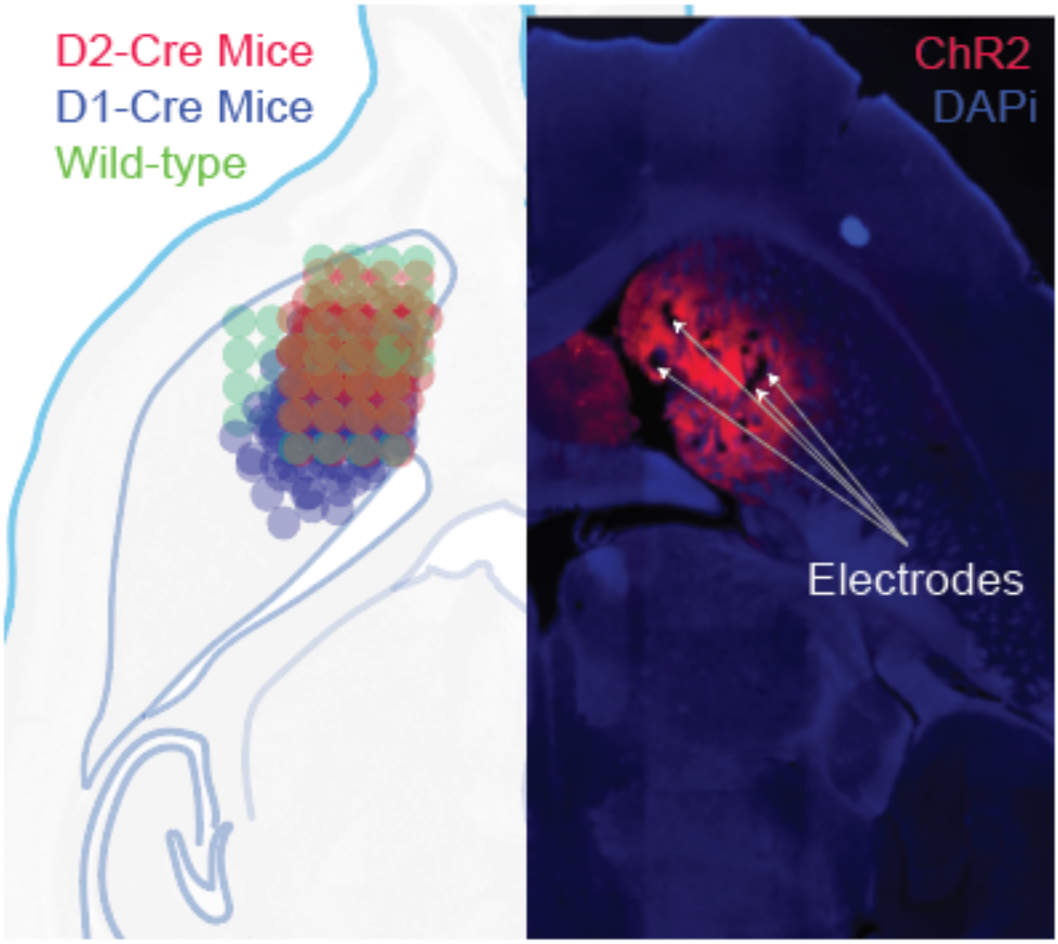

Figure S4: Recording locations in the dorsomedial striatum. Left panel: electrode reconstructions for D2-Cre (red), D1-Cre (blue), and wild-type mice (green). Right panel: reversed image of ChR2 and DAPi stain used for electrode reconstruction (white arrows). Only the left striatum was implanted with electrodes in all animals.

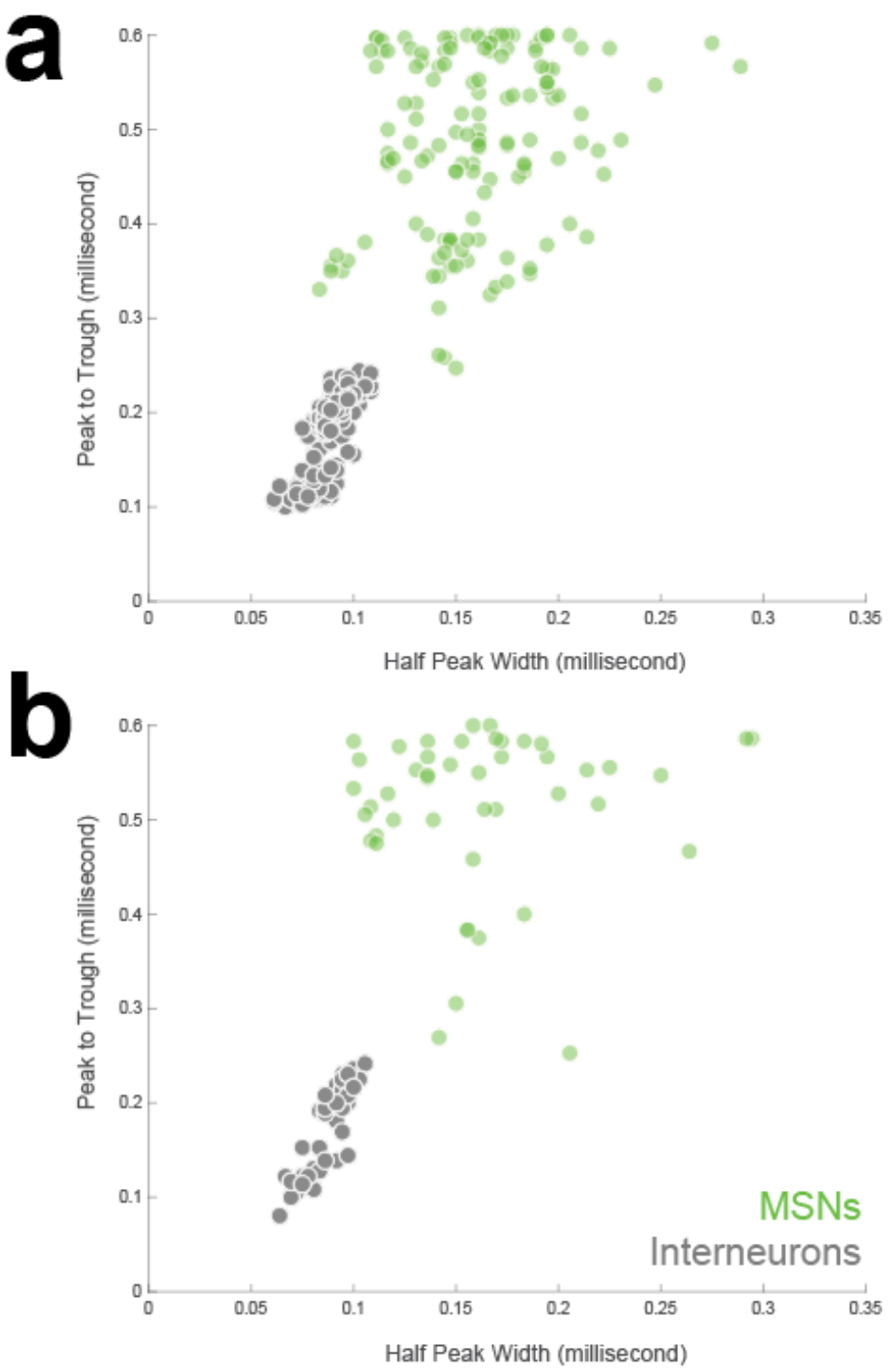

Figure S5: MSN classification by waveform criteria for sessions with a) pharmacology and electrophysiology and b) optogenetic tagging.

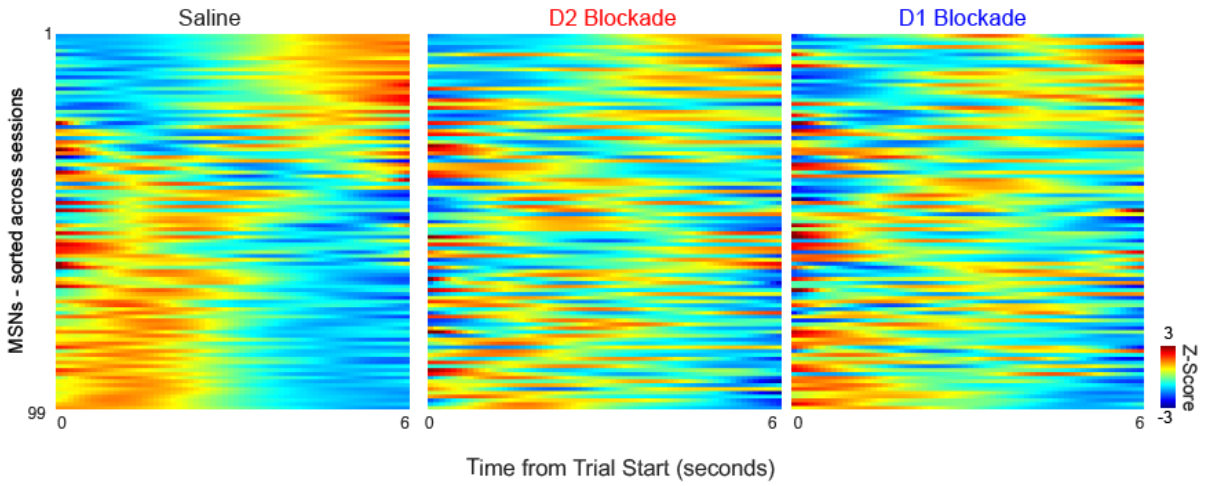

Figure S6: We sorted and identified the same 99 MSNs across saline sessions and sessions with D2 blockade or D1 blockade. Each row is a z-scored peri-event time histogram of MSN activity for all trials during interval timing. Each row is the same neuron identified by waveform and interspike-intervals across saline, D2 blockade, and D1 blockade sessions.

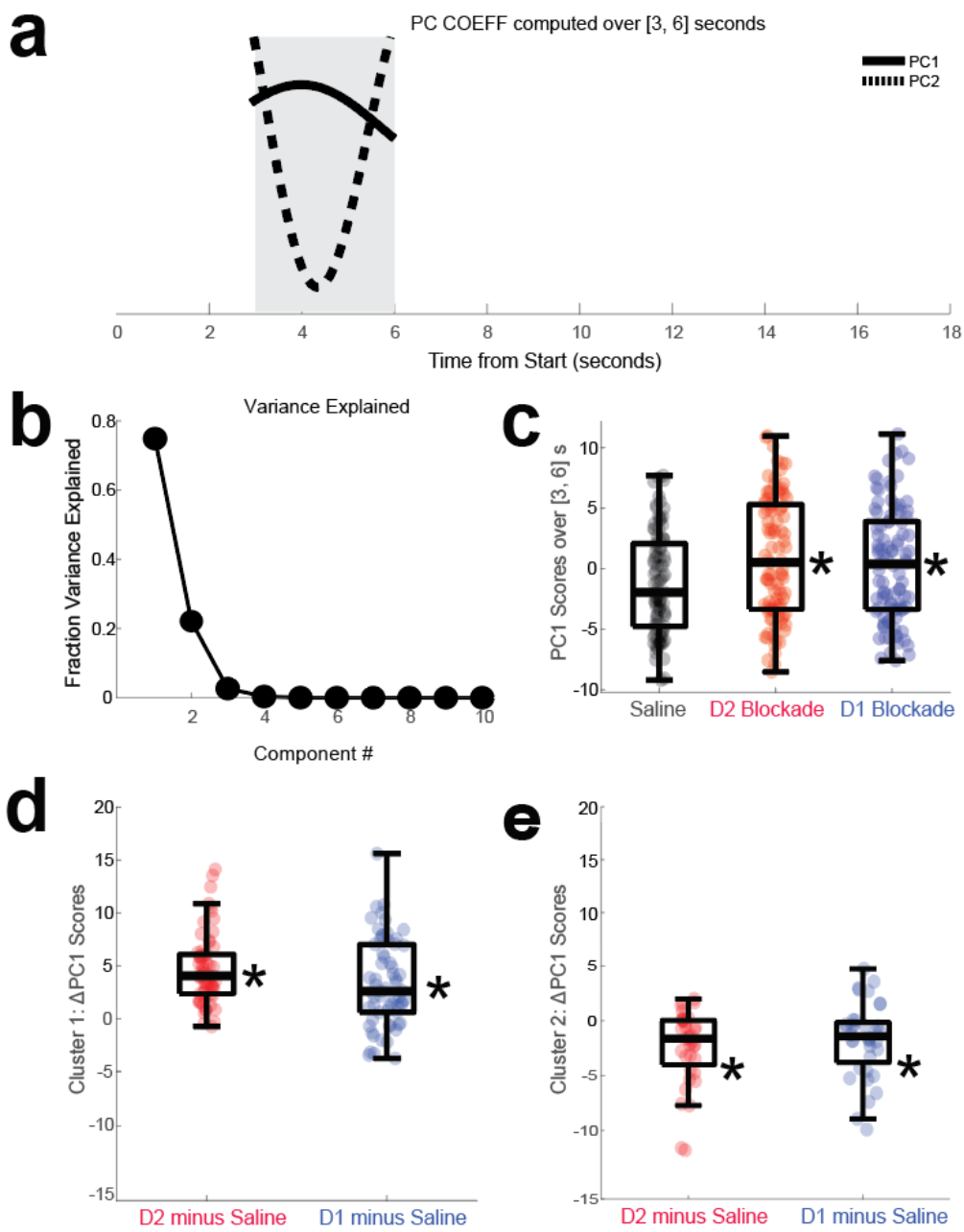

Figure S7: Early-interval ensemble dynamics respond to D2 and D1 blockade. a) We further explored early-interval dynamics by PCA in MSN ensembles with matched sorting among saline, D2 blockade, and D1 blockade (99 neurons; see Fig S6). The matched sorting across sessions enabled paired signed rank analyses. b) Strikingly, the first component (PC1) explained 75% of variance among MSN ensemble dynamics between 3-6 seconds. c) As with dynamics

between 0-6 seconds, PC1 was shifted relative to saline for D2 blockade (signed rank p = 0.000007) and D1 blockade (signed rank p = 0.002). We identified two clusters based on PC1, with cluster 1 (d) loading positively on PC1, and cluster 2 (e) loading negatively on PC1. For cluster 1 in (d), PCs were distinct from saline for D2 blockade (signed rank $p = 3\text{x}10^{-12}$) and for D1 blockade (signed rank $p = 10^{-7}$). For cluster 2 in panel (e), PC1 changes were also distinct for saline for D2 blockade (signed rank p = 0.00008) and for D1 blockade (signed rank p = 0.002).

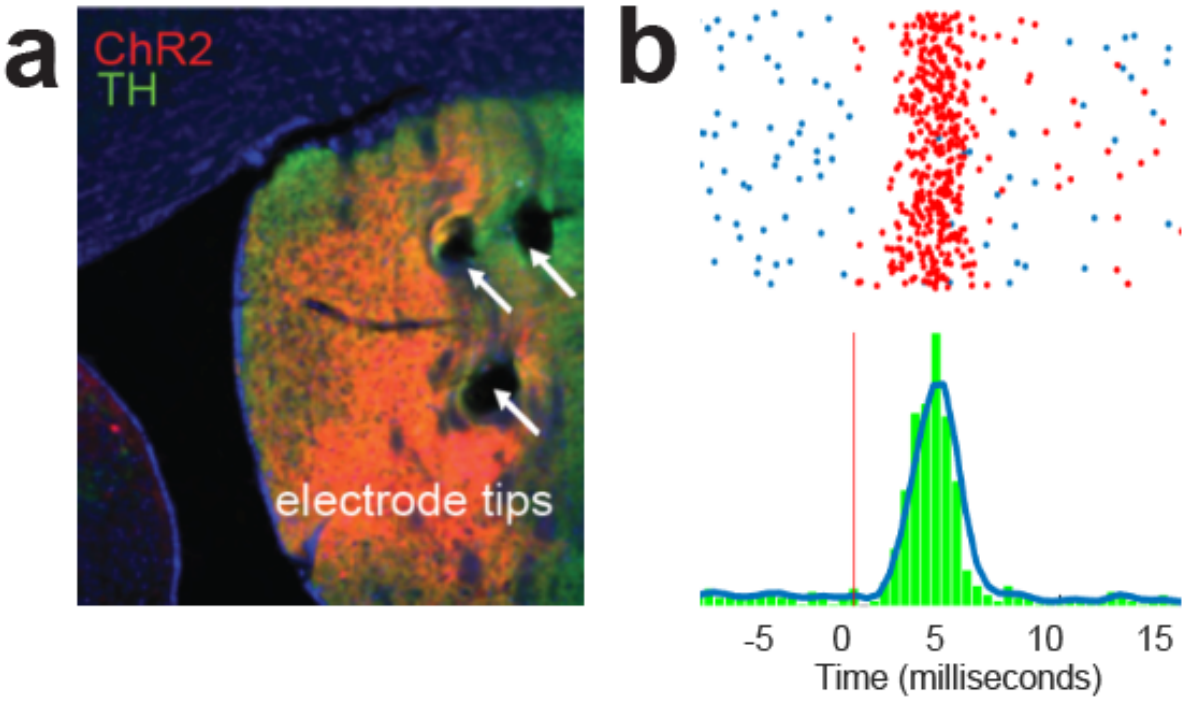

Figure S8: a) Electrode tips in the dorsal striatum, where b) we recorded optogenetically "tagged" neurons that fired action potentials (red) within ≤5 milliseconds of laser onset (red line).

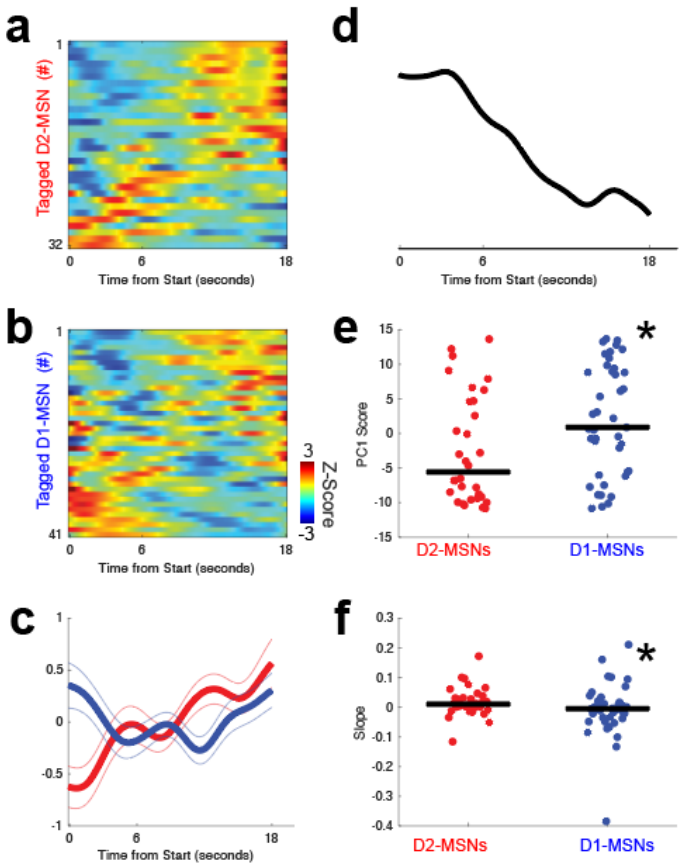

Figure S9: D2- and D1-MSN activity over the whole 18-second interval. a) Peri-event time histograms from D2-MSNs and b) from D1-MSNs over the whole interval. c) We noticed that on average, D2-MSNs tended to ramp up (red), whereas D1-MSNs tended to ramp down (blue). d) Principal component analysis revealed that PC1 exhibited time-dependent ramping over the whole 18-second interval. This component explained ~45% of variance across tagged MSN ensembles. e) Over the whole interval, differences between D2-MSNs and D1-MSNs were captured in PC1, which captures time-dependent ramping (rank sum $p = 0.02$). F) These differences were also captured via differences in a linear slope of firing rate vs time over the whole 18-second interval, with D1-MSNs having a more negative slope (rank sum $p = 0.03$). Data from 32 tagged D2-MSNs in 10 D2-Cre mice and 41 tagged D1-MSNs in 6 D1-Cre mice.

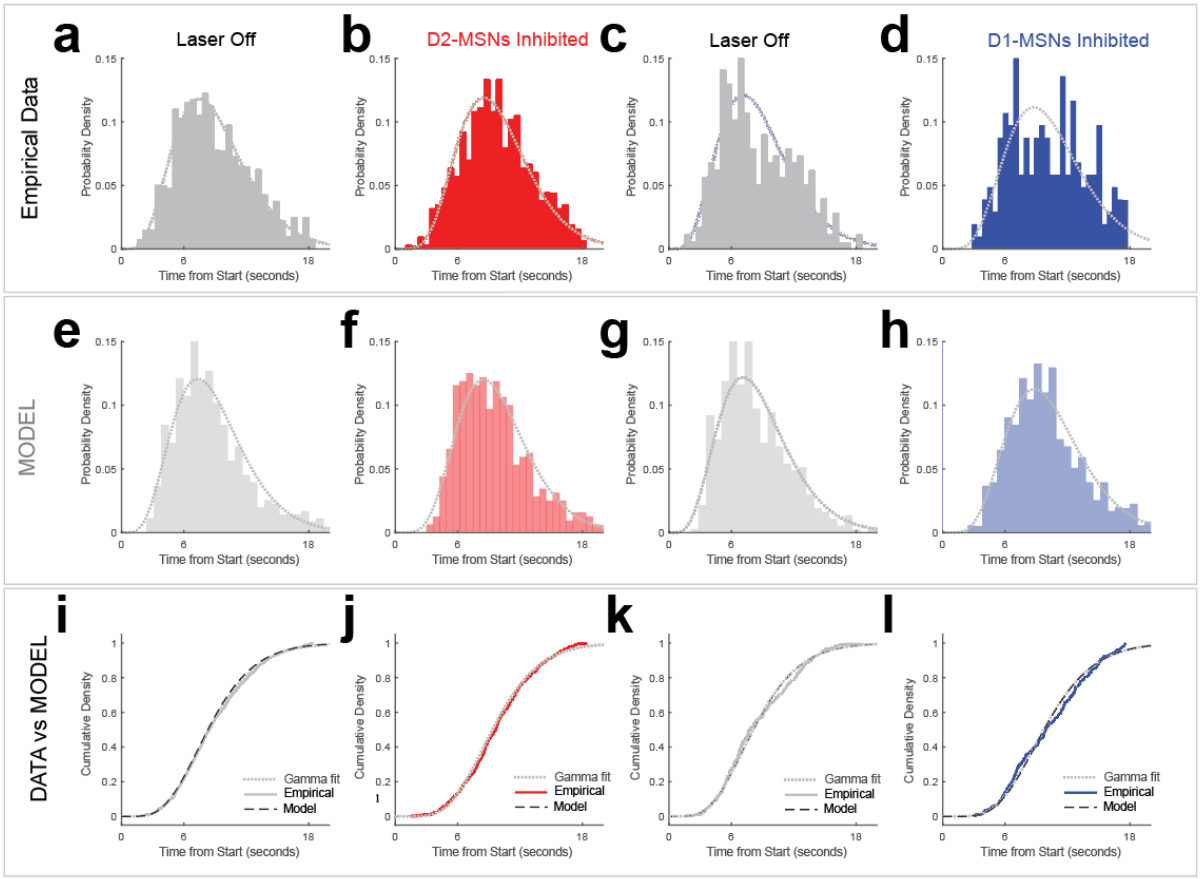

Figure S10: Histograms of behavioral data from D2-Cre mice with a) Laser Off and b) D2-MSN inhibition (red). Data from D1-Cre mice with c) Laser Off and with d) D1-MSN inhibition (blue). e-h) model predictions. i-j) Comparisons of empirical data vs model. All panels: fits for the gamma distribution with dotted circles. Data from 10 D2-Cre mice and 6 D1-mice from Fig 2.

REFERENCES

1. Albin, R. L., Young, A. B. & Penney, J. B. The functional anatomy of basal ganglia disorders. *Trends Neurosci.* **12**, 366–375 (1989).
2. Cruz, B. F. *et al.* Action suppression reveals opponent parallel control via striatal circuits. *Nature* **607**, 521–526 (2022).
3. Cui, G. *et al.* Concurrent activation of striatal direct and indirect pathways during action initiation. *Nature* **494**, 238–242 (2013).
4. Tecuapetla, F., Jin, X., Lima, S. Q. & Costa, R. M. Complementary Contributions of Striatal Projection Pathways to Action Initiation and Execution. *Cell* **166**, 703–715 (2016).
5. Kravitz, A. V. *et al.* Regulation of parkinsonian motor behaviours by optogenetic control of basal ganglia circuitry. *Nature* **466**, 622–626 (2010).
6. Alexander, G. E. & Crutcher, M. D. Functional architecture of basal ganglia circuits: neural substrates of parallel processing. *Trends Neurosci.* **13**, 266–271 (1990).
7. West, A. R. & Grace, A. A. Opposite Influences of Endogenous Dopamine D1 and D2 Receptor Activation on Activity States and Electrophysiological Properties of Striatal Neurons: Studies CombiningIn Vivo Intracellular Recordings and Reverse Microdialysis. *J. Neurosci.* **22**, 294–304 (2002).
8. Jin, X., Tecuapetla, F. & Costa, R. M. Basal ganglia subcircuits distinctively encode the parsing and concatenation of action sequences. *Nat. Neurosci.* **17**, 423–430 (2014).
9. Yun, S. *et al.* Antipsychotic drug efficacy correlates with the modulation of D1 rather than D2 receptor-expressing striatal projection neurons. *Nat. Neurosci.* 1–12 (2023) doi:10.1038/s41593-023-01390-9.
10. Graybiel, A. M. The Basal Ganglia and Cognitive Pattern Generators. *Schizophr. Bull.* **23**, 459–469 (1997).
11. Middleton, F. A. & Strick, P. L. Basal ganglia and cerebellar loops: motor and cognitive circuits. *Brain Res. Rev.* **31**, 236–250 (2000).
12. Wall, N. R., De La Parra, M., Callaway, E. M. & Kreitzer, A. C. Differential Innervation of Direct- and Indirect-Pathway Striatal Projection Neurons. *Neuron* **79**, 347–360 (2013).
13. Averbeck, B. B., Lehman, J., Jacobson, M. & Haber, S. N. Estimates of projection overlap and zones of convergence within frontal-striatal circuits. *J. Neurosci.* **34**, 9497–9505 (2014).
14. Seo, M., Lee, E. & Averbeck, B. B. Action Selection and Action Value in Frontal-Striatal Circuits. *Neuron* **74**, 947–960 (2012).
15. Andreasen, N. C. Understanding the causes of schizophrenia. *N. Engl. J. Med.* **340**, 645–647 (1999).
16. Hinton, S. C. *et al.* Motor timing variability increases in preclinical Huntington's disease patients as estimated onset of motor symptoms approaches. *J. Int. Neuropsychol. Soc.* **13**, 539–543 (2007).
17. Narayanan, N. S. & Albin, R. L. *Cognition in Parkinson's Disease*. (Elsevier, Acad. Press, 2022).
18. Brown, S. W., Collier, S. A. & Night, J. C. Timing and Executive Resources: Dual-Task Interference Patterns Between Temporal Production and Shifting, Updating, and Inhibition Tasks. *J. Exp. Psychol. Hum. Percept. Perform.* (2012) doi:10.1037/a0030484.
19. Parker, K. L., Lamichhane, D., Caetano, M. S. & Narayanan, N. S. Executive dysfunction in Parkinson's disease and timing deficits. *Front. Integr. Neurosci.* **7**, 75 (2013).
20. Merchant, H. & de Lafuente, V. Introduction to the neurobiology of interval timing. *Adv. Exp. Med. Biol.* **829**, 1–13 (2014).
21. Singh, A. *et al.* Timing variability and midfrontal ~4 Hz rhythms correlate with cognition in Parkinson's disease. *NPJ Park. Dis.* **7**, 14 (2021).
22. Merchant, H., Harrington, D. L. & Meck, W. H. Neural Basis of the Perception and Estimation of Time. *Annu. Rev. Neurosci.* **36**, 313–336 (2013).
23. Hamilos, A. E. *et al.* Slowly evolving dopaminergic activity modulates the moment-to-moment probability of reward-related self-timed movements. *eLife* **10**, e62583 (2021).
24. Howard, C. D., Li, H., Geddes, C. E. & Jin, X. Dynamic Nigrostriatal Dopamine Biases Action Selection. *Neuron* **93**, 1436-1450.e8 (2017).

25. Meck, W. H. Neuroanatomical localization of an internal clock: A functional link between mesolimbic, nigrostriatal, and mesocortical dopaminergic systems. *Brain Res.* **1109**, 93–107 (2006).
26. Soares, S., Atallah, B. V. & Paton, J. J. Midbrain dopamine neurons control judgment of time. *Science* **354**, 1273–1277 (2016).
27. Matell, M. S., Meck, W. H. & Nicolelis, M. A. L. Interval timing and the encoding of signal duration by ensembles of cortical and striatal neurons. *Behav. Neurosci.* **117**, 760–773 (2003).
28. Emmons, E. B. *et al.* Rodent medial frontal control of temporal processing in the dorsomedial striatum. *J. Neurosci.* **37**, 8718–8733 (2017).
29. Gouvea, T. S. *et al.* Striatal dynamics explain duration judgments. *eLife* **4**, (2015).
30. Wang, J., Narain, D., Hosseini, E. A. & Jazayeri, M. Flexible timing by temporal scaling of cortical responses. *Nat. Neurosci.* **21**, 102 (2018).
31. Mello, G. B. M., Soares, S. & Paton, J. J. A Scalable Population Code for Time in the Striatum. *Curr. Biol.* **25**, 1113–1122 (2015).
32. Monteiro, T. *et al.* Using temperature to analyze the neural basis of a time-based decision. *Nat. Neurosci.* (2023) doi:10.1038/s41593-023-01378-5.
33. Balci, F. *et al.* Interval timing in genetically modified mice: a simple paradigm. *Genes Brain Behav.* **7**, 373–384 (2008).
34. Bruce, R. A. *et al.* Experience-related enhancements in striatal temporal encoding. *Eur. J. Neurosci.* (2021).
35. Buhusi, C. V. & Meck, W. H. What makes us tick? Functional and neural mechanisms of interval timing. *Nat. Rev. Neurosci.* **6**, 755–765 (2005).
36. Drew, M. R. *et al.* Transient Overexpression of Striatal D2 Receptors Impairs Operant Motivation and Interval Timing. *J. Neurosci.* **27**, 7731–7739 (2007).
37. Stutt, H. R. *et al.* Sex similarities and dopaminergic differences in interval timing. *BioRxiv Prepr. Serv. Biol.* 2023.05.05.539584 (2023) doi:10.1101/2023.05.05.539584.
38. De Corte, B. J., Wagner, L. M., Matell, M. S. & Narayanan, N. S. Striatal dopamine and the temporal control of behavior. *Behav. Brain Res.* **356**, 375–379 (2019).
39. Kamada, T. & Hata, T. Striatal dopamine D1 receptors control motivation to respond, but not interval timing, during the timing task. *Learn. Mem. Cold Spring Harb. N* **28**, 24–29 (2021).
40. Tosun, T., Gur, E. & Balci, F. Mice plan decision strategies based on previously learned time intervals, locations, and probabilities. *Proc. Natl. Acad. Sci. U. S. A.* **113**, 787–792 (2016).
41. Foster, N. N. *et al.* The mouse cortico–basal ganglia–thalamic network. *Nature* **598**, 188–194 (2021).
42. Calabresi, P., Picconi, B., Tozzi, A., Ghiglieri, V. & Di Filippo, M. Direct and indirect pathways of basal ganglia: a critical reappraisal. *Nat. Neurosci.* **17**, 1022–1030 (2014).
43. Bakhurin, K. I. *et al.* Differential Encoding of Time by Prefrontal and Striatal Network Dynamics. *J. Neurosci.* **37**, 854–870 (2017).
44. Narayanan, N. S. & Laubach, M. Delay activity in rodent frontal cortex during a simple reaction time task. *J. Neurophysiol.* **101**, 2859–2871 (2009).
45. Kvitsiani, D. *et al.* Distinct behavioural and network correlates of two interneuron types in prefrontal cortex. *Nature* **498**, 363–366 (2013).
46. Pi, H.-J. *et al.* Cortical interneurons that specialize in disinhibitory control. *Nature* (2013) doi:10.1038/nature12676.
47. Kim, Y.-C. *et al.* Optogenetic Stimulation of Frontal D1 Neurons Compensates for Impaired Temporal Control of Action in Dopamine-Depleted Mice. *Curr. Biol. CB* **27**, 39–47 (2017).
48. Kim, Y. *et al.* Phase-adaptive brain stimulation of striatal D1 medium spiny neurons in dopamine-depleted mice. *Sci. Rep.* **12**, 21780 (2022).
49. Parker, K. L., Chen, K.-H., Kingyon, J. R., Cavanagh, J. F. & Narayanan, N. S. D1-dependent 4 Hz oscillations and ramping activity in rodent medial frontal cortex during interval timing. *J. Neurosci.* **34**, 16774–16783 (2014).
50. Narayanan, N. S. Ramping activity is a cortical mechanism of temporal control of action. *Curr. Opin. Behav. Sci.* **8**, 226–230 (2016).

51. Latimer, K. W., Yates, J. L., Meister, M. L., Huk, A. C. & Pillow, J. W. Single-trial spike trains in parietal cortex reveal discrete steps during decision-making. *Science* **349**, 184–187 (2015).
52. Zylberberg, A. & Shadlen, M. N. Cause for pause before leaping to conclusions about stepping. *bioRxiv* 085886 (2016) doi:10.1101/085886.
53. Luzardo, A., Ludvig, E. A. & Rivest, F. An adaptive drift-diffusion model of interval timing dynamics. *Behav. Processes* **95**, 90–99 (2013).
54. Simen, P., Balci, F., de Souza, L., Cohen, J. D. & Holmes, P. A model of interval timing by neural integration. *J. Neurosci. Off. J. Soc. Neurosci.* **31**, 9238–9253 (2011).
55. Treisman, M. Temporal discrimination and the indifference interval: Implications for a model of the 'internal clock'. *Psychol. Monogr. Gen. Appl.* **77**, 1–31 (1963).
56. Nguyen, Q.-A., Rinzel, J. & Curtu, R. Buildup and bistability in auditory streaming as an evidence accumulation process with saturation. *PLOS Comput. Biol.* **16**, e1008152 (2020).
57. Meck, W. H., Penney, T. B. & Pouthas, V. Cortico-striatal representation of time in animals and humans. *Curr Opin Neurobiol* **18**, 145–52 (2008).
58. Matell, M. S. & Meck, W. H. Cortico-striatal circuits and interval timing: coincidence detection of oscillatory processes. *Cogn. Brain Res.* **21**, 139–170 (2004).
59. Paton, J. J. & Buonomano, D. V. The Neural Basis of Timing: Distributed Mechanisms for Diverse Functions. *Neuron* **98**, 687–705 (2018).
60. Emmons, E. B. *et al.* Rodent Medial Frontal Control of Temporal Processing in the Dorsomedial Striatum. *J. Neurosci.* **37**, 8718–8733 (2017).
61. Toda, K. *et al.* Nigrotectal Stimulation Stops Interval Timing in Mice. *Curr. Biol.* **27**, 3763-3770.e3 (2017).
62. Penney, T. B., Meck, W. H., Roberts, S. A., Gibbon, J. & Erlenmeyer-Kimling, L. Interval-timing deficits in individuals at high risk for schizophrenia. *Brain Cogn.* **58**, 109–118 (2005).
63. Ward, R. D., Kellendonk, C., Kandel, E. R. & Balsam, P. D. Timing as a window on cognition in schizophrenia. *Neuropharmacology* (2011) doi:10.1016/j.neuropharm.2011.04.014.
64. Buhusi, C. V. & Meck, W. H. Differential effects of methamphetamine and haloperidol on the control of an internal clock. *Behav. Neurosci.* **116**, 291 (2002).
65. Friedman, J. H. & Lannon, M. C. Clozapine in the treatment of psychosis in Parkinson's disease. *Neurology* **39**, 1219–1219 (1989).
66. Bergfeld, I. O. *et al.* Deep Brain Stimulation of the Ventral Anterior Limb of the Internal Capsule for Treatment-Resistant Depression: A Randomized Clinical Trial. *JAMA Psychiatry* **73**, 456–464 (2016).
67. Okun, M. S. Deep-brain stimulation for Parkinson's disease. *N. Engl. J. Med.* **367**, 1529–1538 (2012).
68. Gokce, O. *et al.* Cellular Taxonomy of the Mouse Striatum as Revealed by Single-Cell RNA-Seq. *Cell Rep.* **16**, 1126–1137 (2016).
69. Burke, D. A., Rotstein, H. G. & Alvarez, V. A. Striatal Local Circuitry: A New Framework for Lateral Inhibition. *Neuron* **96**, 267–284 (2017).
70. Owen, S. F., Berke, J. D. & Kreitzer, A. C. Fast-Spiking Interneurons Supply Feedforward Control of Bursting, Calcium, and Plasticity for Efficient Learning. *Cell* **172**, 683-695.e15 (2018).
71. Gerfen, C. R. The neostriatal mosaic: compartmentalization of corticostriatal input and striatonigral output systems. *Nature* **311**, 461–464 (1984).
72. F Hernandez, L., Castela, I., Ruiz-DeDiego, I., Obeso, J. A. & Moratalla, R. Striatal activation by optogenetics induces dyskinesias in the 6-hydroxydopamine rat model of Parkinson disease. *Mov. Disord. Off. J. Mov. Disord. Soc.* **32**, 530–537 (2017).
73. Freeze, B. S., Kravitz, A. V., Hammack, N., Berke, J. D. & Kreitzer, A. C. Control of basal ganglia output by direct and indirect pathway projection neurons. *J. Neurosci. Off. J. Soc. Neurosci.* **33**, 18531–18539 (2013).
74. Gong, S. *et al.* Targeting Cre recombinase to specific neuron populations with bacterial artificial chromosome constructs. *J. Neurosci. Off. J. Soc. Neurosci.* **27**, 9817–9823 (2007).

75. Larson, T. *et al.* Mice expressing P301S mutant human tau have deficits in interval timing. *Behav. Brain Res.* **432**, 113967 (2022).
76. Weber, M. A. *et al.* Glycolysis-enhancing α1-adrenergic antagonists modify cognitive symptoms related to Parkinson's disease. *Npj Park. Dis.* **9**, 1–7 (2023).
77. Berke, J. D. Functional properties of striatal fast-spiking interneurons. *Front. Syst. Neurosci.* **5**, 45 (2011).
78. Emmons, E. *et al.* Temporal Learning Among Prefrontal and Striatal Ensembles. *Cereb. Cortex Commun.* **1**, (2020).
79. Emmons, E. B., Kennedy, M., Kim, Y. & Narayanan, N. S. Corticostriatal stimulation compensates for medial frontal inactivation during interval timing. *Sci. Rep.* **9**, 1–9 (2019).
80. Narayanan, N. S. & Laubach, M. Methods for studying functional interactions among neuronal populations. in *Dynamic Brain Imaging* 135–165 (Springer, 2009).
81. Ryan, M. B., Bair-Marshall, C. & Nelson, A. B. Aberrant striatal activity in parkinsonism and levodopa-induced dyskinesia. *Cell Rep.* **23**, 3438–3446 (2018).
82. Shin, J. H., Kim, D. & Jung, M. W. Differential coding of reward and movement information in the dorsomedial striatal direct and indirect pathways. *Nat. Commun.* **9**, 1–14 (2018).
83. Shimazaki, H. & Shinomoto, S. A Method for Selecting the Bin Size of a Time Histogram. *Neural Comput.* **19**, 1503–1527 (2007).
84. Kim, Y.-C. *et al.* Optogenetic stimulation of frontal D1 neurons compensates for impaired temporal control of action in dopamine-depleted mice. *Curr. Biol.* **27**, 39–47 (2017).